DOE/ET-53088-157 IFSR #157

ONSET OF STOCHASTICITY AND THE DIFFUSION APPROXIMATION IN DRIFT WAVES

Wendell Horton

Institute for Fusion Studies
The University of Texas at Austin
Austin, Texas 78712

September 1984

ONSET OF STOCHASTICITY AND THE DIFFUSION APPROXIMATION IN DRIFT WAVES

Wendell Horton
Institute for Fusion Studies
University of Texas at Austin
Austin, Texas 78712

Abstract

The Hamiltonian structure of the $\underset{\sim}{E}\times\underset{\sim}{B}$ drift equations is exploited to describe the onset of stochasticity for test particles in drift waves. In contrast to a longitudinal plasma wave, a drift wave acts over the entire single particle phase space. This feature precludes a simple use of the techniques presently available for predicting the onset of chaos in Hamiltonian systems. For two drift waves a generalized Chirikov overlap criterion is derived. The present work gives conditions on the drift wave spectrum for global stochasticity and the validity of the diffusion approximation.

I. INTRODUCTION

The drift wave instabilities arising from density gradients in a plasma produce anomalous transport of particles across the confining magnetic field as known from laboratory experiments and computer simulations.[1] In fact, it is usual to calculate the effect of the drift waves with quasilinear diffusion coefficients derived from the $\underset{\sim}{E}\times\underset{\sim}{B}$ convection of the particles across the magnetic field.[2,3] In contrast, a single drift wave can only produce a localized convection of the plasma with no net transport. The presence of a small secondary drift wave was shown by Horton[4] to produce stochastic motion along the boundaries of the convective motion giving rise to a net plasma transport. In this work we find conditions for which the drift wave system changes from a localized convection of plasma to a system described by diffusion.

The drift waves considered are low frequency electrostatic waves in which the cross-field particle motion is given by the $\underset{\sim}{E}\times\underset{\sim}{B}$ drift of the guiding center. The $\underset{\sim}{E}\times\underset{\sim}{B}$ motion is Hamiltonian with the canonical momentum being the radial coordinate in the direction of the plasma inhomogeneity and the conjugate coordinate being the spatial coordinate in the direction of symmetry mutually perpendicular to the inhomogeneity and the confining magnetic field. The isolating radial surfaces across which particles do not pass appear as invariant torii[5] in the three dimensional phase space of the Hamiltonian for the drift wave system. We seek to establish the conditions under which these isolating invariant torii break down allowing the radial transport of particles.

In Sec. II we define the canonical coordinates for the Hamiltonian of the guiding center motion in the drift wave system and define the action-angle variables. In Sec. III we give the trajectories of the

integrable single wave system and derive the corresponding Chirikov-overlap condition[5] for the presence of significant stochasticity in the two wave system. We also give a condition for the destabilization of the elliptic fixed points in a special multi-wave system with exact fixed points of the flow. In Sec. IV we analyze the diffusion approximation to the trajectories in the regimes of global stochasticity. Approximate expressions for the diffusion coefficients and the test particle correlation time are derived. Section V contains the discussion and conclusions.

II. TEST PARTICLE MOTION IN DRIFT WAVES

We consider a nonuniform, magnetized plasma with a fixed density gradient $dN/dr=-N/r_n$ and constant radial electric field $E_r=-d\Phi/dr$ in the slab approximation. The nonuniformity of the equilibrium density and potential gives rise to the electron diamagnetic drift velocity $v_{de}=cT_e/eBr_n$ and the E×B drift velocity $v_E=-cE_r/B$ in the symmetry direction $\hat{y}$ perpendicular to the direction $\hat{x}$ of the equilibrium gradient and the direction $\hat{z}$ of the magnetic field $\vec{B}$. The slab supports drift waves with frequency ω and wavenumber $\underset{\sim}{k}=(k_x,k_y)$ related through $\omega-k_yv_E=k_yv_{de}/(1+k_\perp^2\rho^2)$ where $\rho=c(m_iT_e)^{1/2}/eB$ describes the dispersion of the waves due to the polarization of the plasma. The waves are electrostatic with $\underset{\sim}{E}=-\nabla\varphi(x,y,t)$ with a single wave $\underset{\sim}{k}$ of the form $\varphi_{\underset{\sim}{k}}=A_k\sin(k_xx)\cos(k_yy-\omega_{\underset{\sim}{k}}t)$.

In the presence of N drift waves the electrostatic potential is

$$\Phi(x,y,t) = -E_rx + \sum_1^N A_{\underset{\sim}{k}}\sin(k_xx)\cos(k_yy-\omega_{\underset{\sim}{k}}t+\beta_{\underset{\sim}{k}}) \qquad (1)$$

where mode coupling effects[6] are neglected. In writing Eq. (1) the plasma is assumed to be bounded in x and periodic in y with $\underset{\sim}{k}=(\pi n/L_x, 2\pi m/L_y)$.

We consider the motion of a test particle with trajectory $\underset{\sim}{r}(t)=(x(t),y(t))$ moving with the $\underset{\sim}{E}\times\underset{\sim}{B}$ drift velocity in the plasma. We need not specify in detail the type of particle. The test particle may equivalently be taken to be a fluid element with the Lagrangian fluid displacement $\underset{\sim}{\xi}(t)=(x(t),y(t))$ moving with velocity $\underset{\sim}{v}_E=c\underset{\sim}{E}\times\underset{\sim}{B}/B^2$. Thus, the fluid element may be looked on as a fluid particle. For the ions and electrons in a collisionless plasma the approximation of the $\underset{\sim}{E}\times\underset{\sim}{B}$ drift trajectory applies most directly to the motion of the thermal ions since drift waves satisfy the relationship $v_i/L<<\omega<<v_e/L$ where $v_j=(T_j/m_j)^{1/2}$ is the average particle velocity and L is the effective length of the system along the magnetic field line. The electron motion is coupled to the parallel mode structure and is easily made stochastic by overlapping $\omega=k_\parallel v_\parallel$ resonances; however, the ion motion must become stochastic before a net plasma transport occurs.

The motion of the test particle given by $d\underset{\sim}{r}/dt=\underset{\sim}{v}_E$ is an incompressible two dimension flow given by

$$\frac{dx}{dt} = -\frac{c}{B}\frac{\partial\phi(x,y,t)}{\partial y} \tag{2}$$

$$\frac{dy}{dt} = \frac{c}{B}\frac{\partial\phi(x,y,t)}{\partial x} \tag{3}$$

The flow $\dot{x}$, $\dot{y}$ is thus a one-and-a-half dimensional Hamiltonian system with the electrostatic potential $\phi(x,y,t)$ being the Hamiltonian. The appropriate choice for the canonical momentum is the x coordinate and the conjugate coordinate is y. In the equilibrium the coordinate y is cyclical (ignorable)

and the particles are confined to $x(t) = x_o$. In the presence of the waves $\phi = \phi(x,y,t)$ which in general has a complicated structure as shown by the contours of constant $\phi(x,y,t)$ in Fig. 1. Although steep gradients in the Hamiltonian may arise, the physical condition that the energy density W of the waves be a finite fraction of the thermal energy density nT limits the gradients through the condition $W/nT=\int[\phi^2+(\nabla\phi)^2]dxdy<\infty$. In terms of the amplitude spectrum A_k in Eq. (1) the condition of finite W/nT requires $A_{\underset{\sim}{k}}\leq C/|\underset{\sim}{k}|^{2+\varepsilon}$ as $|\underset{\sim}{k}|\to\infty$.

For motions in general potentials it is useful to introduce action-angle variables J, ϑ. With time frozen the motion given by Eqs. (2)-(3) takes place along level contours of $\phi(x,y)$ with the velocity $v_E=\left((\partial_x\phi(x,y))^2+(\partial_y\phi(x,y))^2\right)^{1/2}$. The action J is defined for a given ϕ by

$$J(\phi) = \frac{1}{2\pi}\oint x(y,\phi)dy = \frac{\text{area of } \phi \text{ contour}}{2\pi} \quad . \tag{4}$$

For closed contours the integral (4) becomes $J(\phi) = \int_{y_1}^{y_2} [x^+(y',\phi)-x^-(y',\phi)]dy'/2\pi$ where $y_{1,2}$ are the turning points where $\partial_x\phi=0$ and $x^{\pm}(y,\phi)$ are the two branches of the inverse of $\phi(x,y,t)=\phi$. For open contours the action is $J(\phi)=\int_0^{L_y} x(y,\phi)dy/2\pi$ where L_y is the periodic length of the system.

The generating function S(y,J) for the canonical transformation to action-angle variables (J,ϑ) is

$$S(y,J) = \int_0^y x(y',\phi)dy' \tag{5}$$

with $\phi=\phi(J)$ being the inverse of Eq. (4). The generating function (5) gives $x=(\partial S/\partial y)_J$ and

$$\vartheta = \frac{\partial S(y,J)}{\partial J} = \frac{\partial \phi}{\partial J}\int_0^y \frac{\partial x(y',\phi)}{\partial \phi}\, dy' \quad . \tag{6}$$

Upon using Eq. (3) for $\dot{y}$ and defining the time $t(y)=\int_0^{\ell} d\ell'/v_E=\int_0^y dy'/\dot{y}$ measured along the trajectory, the angle (6) may be written as

$$\vartheta = \frac{\partial \phi}{\partial J}\int_0^y \frac{dy'}{\dot{y}(y',\phi)} = \omega_b(\phi)t(y) \tag{7}$$

where the $\underset{\sim}{E}\times\underset{\sim}{B}$ bounce frequency is defined by

$$\omega_b = \frac{\partial \phi}{\partial J} \quad . \tag{8}$$

The equations of motion in action-angle variables are

$$\frac{d\vartheta}{dt} = \frac{\partial \phi}{\partial J} \quad \text{and} \quad \frac{dJ}{dt} = -\frac{\partial \phi}{\partial \vartheta} \quad . \tag{9}$$

The contours of the potential $\varphi(x,y,t)$ change shape and reconnect on the period of the correlation time $\tau_c=1/\Delta\omega$. When $\omega_b>>\Delta\omega$ the guiding center particles follow the contours of constant J until a separatrix of φ sweeps past them. During the separatrix crossing the particles begin convection in a different potential cell thus making a step $1/\Delta k_\perp$ given by the size of the potential cell. The separatrix crossing process is studied by Kleva and Drake.[7]

III. Integrable Curves for a Single Wave

For a single drift wave in the expansion (1) the equations of motion

$$\dot{x} = k_y A_k \sin(k_x x) \sin(k_y y - \omega_k t + \beta_k) \tag{10}$$

$$\dot{y} = v_E + k_x A_k \cos(k_x x) \cos(k_y y - \omega_k t + \beta_k) \tag{11}$$

are integrable. The integral curves are found by making a canonical transformation to the wave frame x',y' with the generating function

$$F(y,x',t) = x'(y - \frac{\omega_k}{k_y} t) \tag{12}$$

giving $x=\partial F/\partial y=x'$ and $y'=y-(\omega_k/k_y)t$. The Hamiltonian in the wave frame is $\phi'=\phi+\partial F/\partial t$ with

$$\phi'(x',y') = (v_E - \frac{\omega_k}{k_y})x' + A_k \sin(k_x x') \cos(k_y y') \ . \tag{13}$$

To study the integral curves we use phase coordinates $X=k_x x'$, $Y=k_y y'$ and measure time in units of the maximum $\underset{\sim}{E}\times\underset{\sim}{B}$ circulation frequency $\omega_b^o=k_x k_y A_k$ letting $\tau=\omega_b^o t$. The equations for the integral curves are

$$\frac{dX}{d\tau} = \sin X \sin Y \tag{14}$$

$$\frac{dY}{d\tau} = u + \cos X \cos Y \tag{15}$$

with the trapping parameter defined by

$$u = \frac{\omega_k - k_y v_E}{\omega_b^o} \quad . \tag{16}$$

For u=0 all the orbits are closed and are given in terms of the elliptic functions by Horton.[4] For 0<u<1 there are open (passing) and closed (trapped) orbits as shown in Fig. 2 and considered by Hirshman.[8] For u>1 all orbits are open or passing.

For the simplest drift wave dispersion relation the trapping condition $u \leqslant 1$ requires the single wave amplitude to satisfy

$$eA_k/T_e > 1/[k_x r_n(1+k_\perp^2\rho^2)] \sim (\rho/r_n)(1+k_\perp^2\rho^2)^{-1}$$

for waves with $k_x\rho \sim 1$. For comparison with longitudinal trapping we note that the parallel trapping velocity $v_t=(e\phi/m)^{1/2}$ at this amplitude is $v_t^e=(e\phi/m_e)^{1/2} \cong v_e(\rho/r_n)^{1/2}$ for the electrons and negligible for the ions. The electron trapping velocity v_t^e is small compared with $\omega/|k_\parallel|$ for sufficiently small ρ/r_n.

For u<1 the unstable fixed points in a unit cell of phase space as designated by the labels 1,2,3,4 in Fig. 2 are given by $(0,-\pi+\cos^{-1}u)$, $(0,\pi-\cos^{-1}u)$, $(\pi,\cos^{-1}u)$ and $(\pi,-\cos^{-1}u)$, respectively, where $0 \leqslant \cos^{-1}u \leqslant \pi/2$. As $u \to 1$ the unstable pair y_3, y_4 and the two elliptic fixed points at $(\pi \pm \cos^{-1}u, 0)$ coverge to $(\pi,0)$, and the area of the trapped orbits vanishes as $J \alpha (\cos^{-1}u)^2 = (1-u)^2$.

The homoclinic orbits $y_{sx}(t)$ between y_1-y_2 and y_3-y_4 are calculated. The time variation of $y_{sx}(t)$ is given by $\Omega=\omega_b^o(1-u^2)^{1/2}=(\omega_b^{o2}-\tilde{\omega}_k^2)^{1/2}$ for u<1. The dimensionless velocity along y_1-y_2 is $\dot{Y}=u+\cos Y \leqslant 1+u$ and along y_3-y_4 is

$\dot{Y}=u-\cos Y \leqslant 1-u$. The homoclinic orbits $y_{sx}(t)$ along the long side y_1-y_2 is given here by

$$\tan\left(\frac{Y_{sx}(t)}{2}\right) = \begin{cases} \left(\frac{1+u}{1-u}\right)^{1/2} \tanh\left[\frac{\omega_b^o(1-u^2)^{1/2}t}{2}\right], & u<1 \\ \left(\frac{1+u}{u-1}\right)^{1/2} \tan\left[\frac{\omega_b^o(u^2-1)^{1/2}t}{2}\right], & u>1 \end{cases} \tag{17}$$

and is required for the perturbation calculation in the next section. The harmonic motion around the elliptic fixed points $(\pi \pm \cos^{-1}u, 0)$ rotates with frequency $\omega_b(u)=\omega_b^o(1-u^2)^{1/2}$.

A. Two Drift Waves and the Onset of Stochasticity

In the presence of two drift waves $(A_{k_1}, \underset{\sim}{k}_1, \omega_1; A_{k_2}, \underset{\sim}{k}_2, \omega_2)$ we again use the canonical transformation of the type in Eq. (12) to the wave frame of the larger amplitude wave labeled 1. In this transformation the new $x'=k_{1x}x-r\pi$ where $r\pi$ is the r^{th} radial node of the larger amplitude wave. In the following equations we drop the primes on the new coordinates. The two wave Hamiltonian is

$$\Phi = ux + \sin x \cos y + \varphi \sin(kx+\alpha) \cos[q(y-vt)] \tag{18}$$

where u is defined in Eq. (16) and

$$k = \frac{k_{2x}}{k_{1x}} \qquad q = \frac{k_{2y}}{k_{1y}} \qquad \varphi = \frac{A_2}{A_1} \qquad \alpha = \frac{r\pi k_{2x}}{k_{1x}} = r\pi k$$

and

$$v = \frac{\omega_2}{k_{2y}} - \frac{\omega_1}{k_{1y}} \quad . \tag{19}$$

The test particle flow is given by

$$\dot{x} = \sin x \sin y + q\varphi \sin(kx+\alpha) \sin[q(y-vt)]$$

$$\dot{y} = u + \cos x \cos y + k\varphi \cos(kx+\alpha) \cos[q(y-vt)] \quad . \tag{20}$$

To estimate the threshold for the onset of significant stochasticity we calculate the change in the Hamiltonian by perturbation theory along the separatrix of the single wave flow from Eqs. (14)-(17).

The change in the Hamiltonian $\Delta\Phi$ is given by the Melnikov-Arnold integral

$$\Delta\Phi = qv\varphi \sin(\alpha) \int_{-\infty}^{+\infty} \cos[q(Y_{sx}(t)-vt)]dt \tag{21}$$

where $Y_{sx}(t)$ is the trajectory along 1→2 or 3→4. Clearly, $\Delta\Phi=0$ for $\omega''=qv\to 0$ and is exponentially small for $\omega''=qv>>\omega_b^o$. Analysis of the integral (21) is tedious and is given in the Appendix. We summarize the results here.

For small u the homoclinic orbits (17) are approximately

$$Y_{sx}(t) \cong -\frac{\pi}{2} + 2 \tan^{-1}[\exp(\omega_b t)]$$

and the stationary phase condition $\dot{Y}_{sx}(t_s)=v$ is satisfied for real t_s when

the frequency of the perturbation satisfies $\omega_b^o = qv$. This resonance condition gives the the onset of stochasticity criterion

$$\frac{ck_{2y}k_{1x}A_{k1}}{B} \gtrsim |\omega_{k2} - \frac{k_{2y}\omega_{k1}}{k_{1y}}| \tag{22}$$

valid for $A_2 << A_1$. The stochasticity criterion (22) is easily satisfied for long wavelength drift waves. For $0<u<1$ the stationary phase integral is analyzed in the Appendix.

For comparable amplitude drift waves $A_1 \sim A_2$ we find that the threshold condition (22) become generalized to

$$\frac{ck_{1x}A_{k1}}{B} + \frac{ck_{2x}A_{k2}}{B} \gtrsim |\frac{\omega_{k2}}{k_{2y}} - \frac{\omega_{k1}}{k_{1y}}| \ . \tag{23}$$

Condition (23) for the drift wave problem corresponds to the Chirikov overlap criterion $(e\varphi_1/m)^{1/2}+(e\varphi_2/m)^{1/2}>|\omega_1/k_1-\omega_2/k_2|$ for two longitudinal waves.[5] When condition (22) or (23) is satisfied for drift waves stochasticity occurs in bands throughout the single particle phase space in contrast to the longitudinal wave problem.

For $u \lesssim 1$ the analysis is given in the Appendix. The principal change is that the faster velocity along the 1–2 separatrix governs the breakdown of the invariant torii. The condition for a resonance along 1–2 becomes

$$\omega_{b1}(1+u) = \omega_{b1}+\tilde{\omega}_1 \sim qv \ . \tag{24}$$

Away from the resonance conditions (22) or (24) the Melnikov–Arnold integral becomes exponentially small

$$\Delta\Phi \sim \exp[-qv/\omega_{b1}(1+u)]. \qquad (25)$$

In Fig. 3 we show the variation of the stochastic region with varying v for fixed $\varphi=A_2/A_1=0.1$ and u=0.5. The maximum velocity along the homoclinic orbit 1–2 is $\dot{\hat{y}}_{max}=1.5$. For v=0.25 to 0.5 the invariant torii along 1–2 are still preserved. For v=3/4 all the invariant torii appear to be destroyed. At v=3/4 only small islands of stability about the elliptic fixed points remain. For $v \geq \dot{\hat{y}}_{max}=1.5$ approximate invariant torii along 1–2 appear to have returned.

B. Destruction of the Elliptic Fixed Points

We would like to establish conditions under which the primary elliptic fixed points become unstable. To consider this problem we construct from the N wave parameter set $\{\underset{\sim}{k},\omega_{\underset{\sim}{k}},A_k\}$ special Hamiltonians which have an exact elliptic fixed point ($\dot{\hat{x}}^*=0$, $\dot{\hat{y}}^*=0$). Linearizing the equations of motion about x*,y* leads to a generalized Hill equation for the motion of $\delta x(t)$ about the fixed point. The stability condition on the parameters in the Hill equation then lead to the condition for destruction of the last fixed points. The analysis is lengthy so we briefly summarize the results here.

The idea here is to use the result of Schmidt and Bialek[9] that shows for the standard map model of the surface of section that the critical parameters for destabilization of the fixed points give approximations for the destruction of the KAM surfaces and a qualitative understanding of the diffusion approximation.

Consider the stability of neighboring orbits $\delta x(t)$, $\delta y(t)$ about a stable fixed point $k_x x^*=(n+\frac{1}{2})\pi$, $k_y y^*=m\pi$ of the principal wave

$A_k\sin(k_x x)\cos(k_y y)$ to perturbating waves $\sum_i \varphi_i \sin(k_{ix}x)\cos(k_{iy}y-\omega_i t+\beta_i)$. For simplicity we consider the special case u=0 and restrict the large class of perturbating waves $\{\varphi_i, k_{ix}, k_{iy}, \omega_i, \beta_i\}$ such that x*,y* remains an exact equilibrium of the perturbed problem and the frequencies $\omega_i''=\omega_i-k_{iy}(\omega_k/k_y)$ of the perturbations are equal $\omega_i''=\omega''$. The condition that $\dot{x}(x^*,y^*)=\dot{y}(x^*,y^*)=0$ yields the constraints $\sum_i \varphi_i k_{ix} c_i=\sum_i \varphi_i k_{iy} s_i=0$ where $c_i=\cos[(n+\frac{1}{2})k_{ix}/k_x]$ and $s_i=\sin[(n+\frac{1}{2})k_{ix}/k_x]$.

With these restrictions on the perturbation, the equations for the neighboring orbits are

$$\frac{d}{dt}\begin{bmatrix}\delta x\\ \\ \delta y\end{bmatrix} = \begin{bmatrix}\sigma(t)\sum_i c_i\varphi_i k_{ix}k_{iy} & A_k+\gamma(t)\sum_i s_i\varphi_i k_{iy}^2\\ \\ -A_k-\gamma(t)\sum_o s_i\varphi_i k_{ix}^2 & -\sigma(t)\sum c_i\varphi_i k_{ix}k_{iy}\end{bmatrix}\begin{bmatrix}\delta x\\ \\ \delta y\end{bmatrix} \qquad (26)$$

where $\sigma(t)=\sin(\omega''t)$ and $\gamma(t)=\cos(\omega''t)$. Eq. (26) is a Hill stability problem with the equation for $\delta x(t)$ of the form $\delta\ddot{x}+P(t)\delta\dot{x}+Q(t)\delta x=0$ with explicit expressions for P(t) and Q(t) easily worked out. To simply further the analysis presented here we further constrain the perturbing wave parameters to reduce Eq. (26) to a Mathieu equation. For perturbations with $\sum s_i\varphi_i k_{iy}^2=\sum c_i\varphi_i k_{ix}k_{iy}=0$ the problem reduces to

$$\frac{d^2\delta x}{dt^2} + 4A_k(A_k + \cos(2\omega''t)\sum_i s_i\varphi_i k_{ix}^2)\delta x = 0 \qquad (27)$$

which is the Mathieu equation $\delta\ddot{x}+(a-2q\cos 2\tau)\delta x=0$ with $a=(2A/\omega'')^2$ and $q=2A\sum s_i\varphi_i k_{ix}^2/(\omega'')^2$.

For resonant perturbations a=1

$$2\omega_b = 2A_k = |\omega''| \tag{28}$$

the orbits are destabilized for an arbitrarily small amplitude perturbation. For $2\omega_b = 2A < |\omega''|$ (a<1) the neighboring orbits are stable for $-q^2/2 < a < 1-q-q^2/8$. A simple estimate of the stable domain follows from $q_{crit} \leqslant 1-a$ and yields the condition

$$\sum_i s_i \varphi_i k_{ix}^2 < \omega''\left(\frac{\omega''}{2\omega_b} - \frac{2\omega_b}{\omega''}\right) \tag{29}$$

valid for $a^{1/2} = 2\omega_b/|\omega''| \leqslant 1$.

In Fig. 4 we show the results of increasing the amplitude of the perturbing waves acting on a stable fixed point x*,y* of the type analyzed here. In this example the Hamiltonian is

$$\phi(x,y,t) = ux + \sin x \cos y + A\left[\sin k_1(x-x_1^*) - \frac{k_1}{k_2}\sin k_2(x-x_1^*)\right]\cos[q(y-vt)]$$

with $A = A_2/A_1$. Instability of the elliptic fixed point is observed to occur at approximately the conditions given by either Eq. (28) or Eq. (29) are satisfied.

Additional calculations[7,12] for the onset of diffusion have been studied using drift wave maps obtained for an infinite, discrete frequency model $\lim_{N\to\infty} \sum_{-N}^{N} \cos(n\omega_o t) = 2\pi \sum_{n=-\infty}^{+\infty} \delta(\omega_o t - 2\pi n)$ for the broad band frequency spectra[6,10,11] characteristic of drift waves. Although the analysis is

complicated and incomplete global stochasticity and diffusion appears to occur when $K=k_x k_y A_k/\omega_o >> 1$.

Even for simpler systems the transitional region just beyond the critical resonance for the breakdown of the bounding surfaces is difficult to analyze with regard to transport.[13] We do not attempt to analyze the leaky barrier[13] region where a slow, nondiffusive transport is expected.

IV. THE DIFFUSION APPROXIMATION

When the conditions for stochasticity given in Sec. III are satisfied the phase space consists of large regions from stochastic orbits and smaller regions with chains of islands with stable orbits. The presence of small islands of stability in a sea of stochastic orbits is perhaps the generic form of the x-y phase space in drift wave turbulence. In this regime it is an important theoretical assumption to describe the motion by diffusion. The basic condition for diffusion is that the particle moving along its trajectory $\underset{\sim}{r}(t)$ experience a short correlation time τ_c. The intrinsic stochasticity of the system gives rise to the short correlation time.

The definition of the diffusion tensor follows from the formal integration of the equations of motion

$$\underset{\sim}{r}(t) = \int_0^t \underset{\sim}{v}_E \left(\underset{\sim}{r}(t_1), t_1\right) dt_1 \tag{30}$$

along the unknown trajectory $\underset{\sim}{r}(t)$.

Introducing the average $< >$ over the intial conditions $\underset{\sim}{r}(t=0)=\underset{\sim}{r}_o$ in the stochastic region of phase space the diffusion tensor is defined through the limit

$$\langle \underset{\sim}{r}^2(t)\rangle = \lim_{t/\tau_c\to\infty} \int_0^t dt_1 \int_0^t dt_2 \langle \underset{\sim}{v}_E(t_1)\underset{\sim}{v}_E(t_2)\rangle = 2t \underset{\approx}{D} . \tag{31}$$

The approximation $\langle \underset{\sim}{r}^2(t)\rangle \simeq 2t\underset{\approx}{D}$ is expected to be valid when the correlation time τ_c along the orbit is short compared with nominal orbital period $1/\omega_b$ where $\omega_b = c\, k_x k_y \phi_{\underset{\sim}{k}}/B$. In terms of τ_c the integral in Eq. (31) is estimated by $D \simeq \langle v_E^2\rangle \tau_c$. For a general Hamiltonian $\Phi(x,y,t)$ we define the action J and bounce frequency ω_b through Eqs. (4) and (8). The dimensionless parameter determining the nonlinear regime of the system is

$$R = \omega_b \tau_c \cong \langle v_E^2\rangle^{1/2} \tau_c/\delta \tag{32}$$

where τ_c is the correlation time and δ the spatial correlation scale of the stochastic Hamiltonian $\varphi(x,y,t)$. We assume here that $\varphi(x,y,t)$ is essentially isotropic in the x-y plane. The quasilinear regime is defined by $R \ll 1$ where Eqs. (30)-(31) give $D = \langle v^2_E\rangle \tau_c = (\delta^2/\tau_c) R^2$. The value of R determines the average rotation of the phase in action angle variables according to Eq. (7).

In the strongly nonlinear regime $R \gg 1$ the trajectories make many orbital rotations in one correlation and thus the action integral J is a good adiabatic invariant. In this regime there is a diffusion which occurs in the action variable $\langle \Delta J^2\rangle = D_J t$ for time scales long compared with the orbital period $1/\omega_b$. In this regime a fraction of the particles cross the moving separatrices in each correlation time.[7] By crossing the separatrix they circulate in different convective cell moving across the a distance δ when averaged over ω_b. The maximum rate of this diffusion is $D_m = \delta^2/\tau_c$. From computer experiments with two drift waves with $\underset{\sim}{k}_1 \times \underset{\sim}{k}_2 \cdot \hat{z} \neq 0$ and $k_y \Delta(\omega_k/k_y) \sim \omega_k$ we find a maximum of the diffusion coefficient for $R \sim 1$.

To calculate the diffusion coefficient in terms of the Hamiltonian $\Phi(x,y,t)$ we introduce a statistical description of the test particle distribution function

$$n(\underset{\sim}{x},t) = \sum_{j=1}^{N_T} \delta(\underset{\sim}{x}-\underset{\sim}{r}_j(t,\underset{\sim}{r}_o)) \tag{33}$$

for N_T identical test particles with different initial conditions $\underset{\sim}{r}_o$. The initial coordinates are given by the probability distribution $P(\underset{\sim}{r}_o)$ with $<n(\underset{\sim}{x},t)>=N_T\int d\underset{\sim}{r}_o P(\underset{\sim}{r}_o)\delta(\underset{\sim}{x}-\underset{\sim}{r}_1(t,\underset{\sim}{r}_o))$ with the initial value $<n(\underset{\sim}{x},t=0)>=N_T P(\underset{\sim}{x})$.

A simple example is shown in Fig. 5 where the initial distribution has N_T=50 particles uniformly distributed in y at $X=k_{x1}x=\pi/4$ as shown in Fig. 5a. Figures 5(b)-(f) show the surface of sections for the two drift wave system

$$\varphi(x,y,t) = ux+\Phi_1[\sin x \cos y + \cos kx \cos q(y-vt)]$$

for increasing values of Φ_1 with the parameters u=0, k=v=1, and q=2. The critical condition (23) for the onset of global stochasticity gives $\Phi_{1c}=kv/2=0.5$. At $\Phi_1=0.4$ in Fig. 5(b) the flow is stochastic around the boundaries of the convective cells. At $\Phi_1=0.5$ in Fig. 5(c) the last invariant surfaces are breaking up. At $\Phi_1=1.0$ in Fig. 5(d) there are no more invariant surfaces and no fixed points with islands visible on this scale. At $\Phi_1=2.0$ in Fig. 5(e) the system appears ergodic for the 200 iterations used in these figures. At $\Phi_1=7$ in Fig. 5(f) adiabatic islands produced by the rapid convection have emerged in the flow. (For irrational k, q values the adiabatic islands disappear). Figure 6 shows the diffusion coefficient D_x for this flow computed from Eq. (31) and averaged over the N_T test particles.

For very large Φ_1 the white adiabatic regions of Fig. 5(f) expand to form a pattern of nearly regular convective cells and the diffusion is reduced. To analyze $\Phi_1 \to \infty$ let $t' = \Phi_1 t$ then $\varphi(x,y,t) \to \varphi'(x,y,t')$ with parameters $\Phi_1' = 1$, $u' = u/\Phi_1$, $v' = v/\Phi_1$ and $k' = k$, $q' = q$. In the limit $\Phi_1 \to \infty$, $u' = v' = 0$ so that $\varphi' \to \varphi'(x,y)$ is integrable and the diffusion coefficient vanishes. Rather large values of Φ_1 are required, however, to reach this regime as seen from Figs. 5 and 6.

The distribution of test particles satisfies the conservation law

$$\frac{\partial n(\underset{\sim}{x},t)}{\partial t} = -\underset{\sim}{v}_E \cdot \nabla n = -\frac{c}{B}\left(\frac{\partial \phi}{\partial x}\frac{\partial n}{\partial y} - \frac{\partial \phi}{\partial y}\frac{\partial n}{\partial x}\right) . \tag{34}$$

since $\nabla \cdot \underset{\sim}{v}_E = 0$. In the diffusion approximation the average distribution $\langle n \rangle$ satisfies

$$\partial_t \langle n \rangle = -\nabla \cdot \langle n \underset{\sim}{v}_E \rangle \cong \underset{\approx}{D} : \nabla^2 \langle n \rangle \tag{35}$$

whose solution gives $\langle \underset{\sim}{r}^2 \rangle = \int \underset{\sim}{x}^2 \langle n \rangle d\underset{\sim}{x} = 2\underset{\approx}{D}t$ consistent with Eq. (31).

To calculate the correlation function $\langle n \underset{\sim}{v}_E \rangle$ in Eq. (35) we find the response $\delta n_{\underset{\sim}{q}\Omega}$ to a gradient $\nabla \langle n \rangle$ through the renormalized perturbation expansion[14] of Eq. (34). Following the well known calculation for the renormalized response function $g_{\underset{\sim}{q}\Omega} = (\Omega - q_y v_E + i\nu_{\underset{\sim}{q}})^{-1}$ we obtain

$$\delta n_{\underset{\sim}{q}\Omega} = \frac{c}{B} \frac{\Phi_{\underset{\sim}{q}\Omega} \hat{z} \times \underset{\sim}{q} \cdot \nabla \langle n \rangle}{\Omega - q_y v_E + i\nu_{\underset{\sim}{q}}} \tag{36}$$

with $\nu_{\underset{\sim}{q}}$ given by

$$\nu_{\underset{\sim}{q}} = -\mathrm{Im}\,\frac{c^2}{B^2}\sum_{\underset{\sim}{k}_1\omega_1}\frac{(\underset{\sim}{k}_1\times\underset{\sim}{q}\cdot\hat{z})^2<|\phi_{\underset{\sim}{k}_1\omega_1}|^2>}{\omega_1-k_{1y}v_E+i\nu_{\underset{\sim}{k}1}} \quad . \tag{37}$$

From Eq. (36) the flux $<n\underset{\sim}{v}_E>$ is calculated as

$$<n\underset{\sim}{v}_E> = \frac{c}{B}\sum_{\underset{\sim}{q}} i\hat{z}\times\underset{\sim}{q}\phi_{\underset{\sim}{q}}\delta n_{\underset{\sim}{q}} = -\underset{\approx}{D}\cdot\nabla<n>$$

where

$$\underset{\approx}{D} = -\frac{c^2}{B^2}\,\mathrm{Im}\sum_{\underset{\sim}{q}\Omega}\frac{(\hat{z}\times\underset{\sim}{q})^2<|\phi_{\underset{\sim}{q}\Omega}|^2>}{\Omega-q_yv_E+i\nu_{\underset{\sim}{q}}} \quad . \tag{38}$$

Equations (37) and (38) determine the diffusion tensor from the spectral components of the Hamiltonian $\phi(x,y,t)=\sum_{\underset{\sim}{k}\omega}\phi_{\underset{\sim}{k}\omega}\exp(i\underset{\sim}{k}\cdot\underset{\sim}{x}-i\omega t)$.

The theory leading to $\underset{\approx}{D}$ is not exact but is an infinite order perturbation expansion in R. The terms retained and neglected in the summations leading to (37) and (38) are given in Horton and Choi.[14] In the renormalized perturbation expansion the value of $R\sim ckq\varphi_k/B\nu_k$ is limited even for large ϕ_k since the decorrelation rate increases with ϕ_k according to Eq. (37).

The equations for $\underset{\approx}{D}$ contain two limiting cases. In the presence of many small amplitude waves the correlation time in Eq. (37) is determined by the dispersion $\Delta(\Omega-q_yv_E)>\nu_q$ rather than the nonlinearity. The diffusion becomes the quasilinear diffusion

$$\underset{\approx}{D} \simeq \underset{\approx}{D}^{ql} = <\underset{\sim}{v}_E^2>\tau_c^{ql}$$

with

$$\tau_c^{q\ell} = <|\Omega - q_y v_E|^{-1}> \sim 1/(\Delta\Omega - \Delta q_y v_E) .$$

As R approaches unity the nonlinear decorrelation $\nu_{\underset{\sim}{q}} \geq \Delta(\Omega - q_y v_E)$ determines the rate of decorrelation and $D < D^{q\ell}$. Although not exact, the equation for $\nu_{\underset{\sim}{q}}$ can be approximated to give the estimate

$$\nu_{\underset{\sim}{q}} \simeq \left(\frac{c^2}{B^2} \sum_{\underset{\sim}{k}_1 \omega_1} (\underset{\sim}{k}_1 \times \underset{\sim}{q} \cdot \hat{z})^2 <|\phi_{k_1 \omega_1}|^2>\right)^{1/2} = <\omega_b^2>^{1/2} \simeq <(\underset{\sim}{q} \cdot \underset{\sim}{v}_E)^2>^{1/2} \quad (39)$$

for the nonlinear decorrelation rate for $R \lesssim 1$. With the nonlinear decorrelation rate $\nu_q \sim <\omega_b^2>^{1/2}$ the diffusion coefficient becomes

$$\underset{\approx}{D} = \frac{c^2}{B^2} \sum_{\underset{\sim}{q}\Omega} \frac{(\hat{z} \times \underset{\sim}{q})^2 |\phi_{\underset{\sim}{q}\Omega}|^2}{\nu_{\underset{\sim}{q}}} \simeq <v_E^2>^{1/2} / <k> . \quad (40)$$

with the maximum diffusion occuring for R~1 where

$$D_{max} \sim \frac{\delta^2}{\tau_c} \quad \text{at} \quad R \sim 1. \quad (41)$$

For the simple example in Figs. 5 and 6, the predictions of Eq. (39) and (40) are that $\tau_c^{q\ell} = 1/qv = 0.5$ with $D_x^{q\ell} = c_1 \phi_1^2$ for $\phi_{1c} << \phi_1 < \phi_{1t}$ and $\tau_c = 1/\nu_q \simeq 3/kq\phi_1$ with $D_x = c_2 \phi_1$ for $\phi_1 > \phi_{1t}$. The transition occurs where $\nu_q \simeq kq\phi_1/3 \sim qv$ or at $\phi_{1t} \simeq 3$. The measured scaling of D_x with ϕ_1 is shown in Fig. 6.

For R>>1 we find the diffusion is less than D_{max} which we interpret as due to the adiabatic invariance of J in regime $\omega_b\tau_c>>1$.

The scaling of D for large Φ_1 reported here appears to contradict the weakly increasing $\Phi_1^{1/2}$ dependence found by Kleva and Drake.[7] The difference may lie in the choice of the $\varphi_{\underset{\sim}{k}}$ spectrum considered in their work and here. An exact understanding of the discrepancy requires further analysis.

The well known[1] scale for anomalous transport produced by drift wave turbulence follows from D_{max} with the estimate of the cross-scale correlation distance as $\delta\sim 1/\langle k_x^2\rangle^{1/2}\sim\rho$ and the correlation time as $\tau_c=1/\Delta\omega_k\simeq r_n/c_s$. The drift wave diffusion coefficient is then $D_{dw} = \tau_c^{-1}/\langle k_x^2\rangle\sim(\rho/r_n)(cT_e/eB)$ times a function of order unity containing the other dimensionless parameters of the system.

V. SUMMARY AND CONCLUSIONS

The $\underset{\sim}{E}\times\underset{\sim}{B}$ flow of plasma is a d=1-1/2 dimensional Hamiltonian system. In contrast to the Hamiltonian for motion in longitudinal waves where localized velocity resonances occur, each wave in the $\underset{\sim}{E}\times\underset{\sim}{B}$ system acts over the entire single particle phase space producing a two dimensional array of trapping cells. In the presence of a second perturbing wave stochasticity of the motion sets in along the web of critical contours given by $\omega_b(\Phi)=\partial\Phi/\partial J\sim ck_xk_y\Phi/B\sim 0$ which define the separatricees of the integrable single wave system.

For the two wave system we derive conditions (22)-(24) for the onset of stochasticity as shown, for example, in Fig. 3. The onset of stochasticity is derived from an analysis of the Melnikov-Arnold integral for the effect of perturbations along the critical flow contours defined by $\omega_b(\Phi)=0$.

The onset of stochasticity guarantees the presence of anomalous

transport but is not sufficient for the diffusion approximation to be valid. To find conditions for the complete stochastization of phase space we follow the procedure of Schmidt and Bialek[9] of finding the parameters for perturbations to destabilize robust stable fixed points.

In Sec. IIIB we derive the condition for destabilization of special fixed points in the multi-wave Hamiltonian with the wave parameters $\{\phi_i, \underset{\sim}{k}_i, \omega_i\}$ chosen to provide an exact stable fixed point at finite values of the amplitudes ϕ_i. With a given frequency range $\Delta\omega=\omega''$ the condition (29) derived for destabilization of the flow is approximately $\tilde{\omega}_b \gtrsim \Delta\omega$ where $\tilde{\omega}_b$ is a circulation frequency in the perturbing waves. Figure 4 shows how the entire phase space becomes stochastic as this condition is satisfied. In this regime of global stochasticity the phase space is mixing and the average motion is described by diffusion $\langle \underset{\sim}{r}^2(t)\rangle = 2\underset{\approx}{D}t$.

In the globally stochastic regime the diffusion process takes on different forms depending on the strength of the convecton $\tilde{\omega}_b=\langle\omega_b^2\rangle^{1/2}$ and the correlation time τ_c through the parameter $R=\tilde{\omega}_b\tau_c=\tilde{v}_E\tau_c/\delta$ where $\tilde{v}_E=\langle v_E^2\rangle^{1/2}$ and δ is the spatial correlation distance of $\varphi(x,y,t)$. For $R<1$ the diffusion occurs in the x,y coordinates and is derived in Sec. IV from renormalized turbulence theory. Summation of the secular contributions to perturbation theory gives the approximate formulas (39) and (40) for the nonlinear correlation time and the diffusion coefficient valid for $R \lesssim 1$. For $R \lesssim 1$ the diffusion coefficient increases as $D \simeq \langle v_E^2\rangle^{1/2}\delta$ reaching the maximum $D_{max}=\delta^2/\tau_c$ at $R=1$.

For $R>>1$ the convection is rapid compared with the rate of decorrelation. In this regime the motion occurs as a shown in Fig. 1 with the level contours of $\Phi(x,y,t)$ changing slowly on the time scale τ_c. The

adiabatic invariance of the action forces most of the diffusion to occur from the process of trapping and detrapping.[7]

The motion studied in this work is that of test particles in a two dimensional incompressible flow. The test particles may be actual charged particles of the collisionless plasma or the Lagrangian motion of fluid elements with a velocity $\underset{\sim}{v}=(-\partial_y\phi,\partial_x\phi)$ given by the stream function $\phi(x,y,t)$. For drift waves with $T_i<<T_e$ the distinction between the fluid and ion motion is immaterial. For other systems, such as ideal MHD, the test particles must be viewed as elements of a fluid field such as mass density. In this regime the fluid particle does not have the same stream function Hamiltonian as the charged particles due to diamagnetic and finite Larmor radius currents.

Finally, we point out that the test particle may also be an element of any physical quantity F convected $d_tF=\partial_tF+\underset{\sim}{v}\cdot\nabla F=0$ by a two dimensional incompressible flow. Immediate applications are the convection of the pressure $d_tp=0$ in pressure gradient driven instabilities[4], the convection of vorticity $d_t\omega=0$ in sheared flows, and the convection of magnetic flux $d_t\psi=0$ in tearing modes. In these examples, the anomalous transport and diffusion coefficient derived here produce an anomalous thermal conductivity, anomalous viscosity and anomalous resistivity, or magnetic diffusivity, respectively. In this context, the maximum rate of diffusion $D_m\simeq\delta^2/\tau_c$ derived here for the test particle motion is the same as the widely used mixing length estimate for the rate of anomalous transport. The mixing length level of saturation for drift wave turbulence $\lambda_x|dn/dx|\sim\delta n$ is, in fact, the R=1 regime with $\delta=\lambda_x$ and $\tau_c=1/\Delta\omega$.

Acknowledgments

The author expresses his thanks to Drs. George Schmidt and D. F. Escande for numerous stimulating discussions and to Lee Leonard for the computational analysis of the problem.

We gratefully acknowledge the hospitality of the Aspen Center for Physics where the work was initiated.

This work was supported by the Department of Energy Grant #DE-FG05-80ET-53088.

References

1. W. Horton, "Drift Wave Turbulence and Anomalous Transport", Handbook of Plasma Physics Vol. II, Eds. M. N. Rosenbluth and R. Z. Sagdeev, (Elsevier Science Publishers, 1984), pp. 383-449.
2. A. A. Galeev and R. Z. Sagdeev, "Nonlinear Plasma Theory", in Reviews of Plasma Physics, Vol. 7, Ed. M. A. Leontovich (Consultants Bureau, New York, 1979) pp. 103-114.
3. B. B. Kadomtsev, Plasma Turbulence (Academic Press, London) 1965.
4. W. Horton, Plasma Physics 23, 1107 (1981).
5. B. V. Chirikov, Phys. Reports 52, 263 (1979).
6. P. W. Terry and W. Horton, Phys. Fluids 26, 106 (1983).
7. R. G. Kleva and J. F. Drake, Univ. of Maryland Preprint UMLPF 84-011 (1983).
8. S. P. Hirshman, Phys. Fluids 23, 562 (1980).
9. G. Schmidt and J. Bialek, Physica 5D, 397 (1982).
10. E. Mazzucato, Phys. Rev. Letts. 36, 792 (1976) and 48, 1828 (1982).
11. C. M. Surko and R. E. Slusher, Phys. Rev. Lett. 36, 1747 (1976) and 40, 400 (1978).
12. W. Horton, D. F. Escande, and G. Schmidt, Bull. Am. Phys. Soc. 28, 1209 (1983).
13. R. S. MacKay, J. D. Meiss and I. C. Percival, Phys. Rev. Lett. 52, 697 (1984).
14. W. Horton and D. Choi, Phys. Reports 49, 273 (1979).

APPENDIX

Evaluation of the Melnikov–Arnold Integral

The criterion for the onset of stochasticity is based on the magnitude of integral (21) that gives the change in the Hamiltonian $\Delta\varphi$ along the homoclinic orbit in Eq. (17). The last barrier to the onset of stochasticity is given by the orbit connecting the hyperbolic fixed points labeled 1 and 2 in Fig. 2. The equation of motion of the homoclinic orbit is $dy/dt = \omega_b^o(\cos y+u)$, where $\omega_b^o = ck_x k_y \varphi/B$ and $u = (\omega_k - k_y v_E)/\omega_b^o$. For $0 \leqslant u \leqslant 1$ we define the functions of u

$$\omega_b = \omega_b(u) = \omega_b^o(1-u^2)^{1/2} \quad \text{and} \quad R = \left(\frac{1-u}{1+u}\right)^{1/2} \tag{A1}$$

with $0 \leqslant R \leqslant 1$.

The orbit in Eq. (17) may be solved for t as a function of y:

$$\tau = \omega_b t = \ell n \left[\frac{1+R\tan(y/2)}{1-R\tan(y/2)}\right] , \tag{A2}$$

and the mapping of the t to y plane constructed. The real t axis $(-\infty,+\infty)$ maps to $[y_1,y_2]$ with $\tan(y_1/2) = -1/R$ and $\tan(y_2/2) = 1/R$. The imaginary y axis $(-i\infty, i\infty)$ maps to the interval $(-it_1, it_1)$ with $t_1 = (2/\omega_b)\tan^{-1}R$. The orbit and mapping is invariant to $t \to -t$ and $y \to -y$.

The integral in Eq. (21) reduces to

$$A_k(\Omega,u) = \int_{-\infty}^{+\infty} e^{iky(t)-i\omega''t}dt \ , \qquad (A3)$$

where k is the ratio of the wavenumbers and ω'' is the frequency of the second wave. We consider the case where ω'' and k are positive, real numbers. The function $\exp(-i\omega''t)$ is entire and exponentially decaying for $\mathrm{Im}(t) < 0$. The function $\exp[iky(t)]$ has branch points along the imaginary t axis found by solving Eq. (A2) for exp(iy) to obtain

$$e^{iy(t)} = \frac{1+iR-(1-iR)e^{\tau}}{(1+iR)e^{\tau}-1+iR} \ . \qquad (A4)$$

The simple poles of Eq. (A4) are at $t_n = i(2\pi n-2\tan^{-1}R)/\omega_b$ and are the branch points of the integrand shown in Fig. 7.

The dominant contribution to Eq. (A3) arise from the resonance at the point of stationary phase where

$$\frac{dy}{dt} = \omega_b^o(u+\cos y) = \frac{\omega''}{k} \ . \qquad (A5)$$

We define y_s, Ω and $\tilde{\Omega}$ by

$$\cos y_s = \frac{\Omega}{k} - u = \frac{\tilde{\Omega}}{k} \quad \text{and} \quad \Omega = \frac{\omega''}{\omega_b^o} \ .$$

There are three cases for evaluating Eq. (A3):

$$\text{(i)}\quad y_s = \pm\cos^{-1}(\tilde{\Omega}/k) \quad \text{for} \quad -k < \tilde{\Omega} < k$$

$$\text{(ii)}\quad y_s = 0 \quad \text{and} \quad t_s = 0 \quad \text{for} \quad \tilde{\Omega} = k$$

$$\text{(iii)}\quad y_s = i\beta_s \quad \text{with} \quad \beta_s = \pm\cosh^{-1}(\tilde{\Omega}/k) \quad \text{for} \quad |\tilde{\Omega}| > k \ .$$

We calculate $\ddot{y} = \omega_b^o \sin y\dot{y} = (\omega_b^o\omega''/k)\sin y_s$ at the points of stationary phase and determine the contours of steepest descent shown as contours C_1, C_2, and C_3 in Fig. 7 for cases (i), (ii), and (iii), respectively.

(i) For $|\tilde{\Omega}| < k$, the points of stationary phase occur at $\pm t_s$ on the real axis and the dominant contribution is

$$A_k(\Omega,u) \cong \frac{2\cos(\psi_s-\pi/4)}{\omega_b^o}\left[\frac{2\pi}{\Omega(1-\tilde{\Omega}^2/k^2)^{1/2}}\right]^{1/2} , \qquad \text{(A6)}$$

where

$$\psi_s = k\cos^{-1}\left(\frac{\tilde{\Omega}}{k}\right) - \frac{\omega}{\omega_b}\ln\left[\frac{k+\tilde{\Omega}+R(k^2-\tilde{\Omega}^2)^{1/2}}{k+\tilde{\Omega}-R(k^2-\tilde{\Omega}^2)^{1/2}}\right] .$$

The contribution (A6) increases as $\tilde{\Omega} \to k$ until the contribution from $\ddot{y}^o(t_s)$ is greater than from $\ddot{y}(t_s)$.

(ii) For $\tilde{\Omega}^2 \simeq k^2$ approximation (A6) fails and is replaced by

$$A_k(\Omega,u) \simeq \int_{-\infty}^{+\infty} dt\ e^{-i\omega_b^{o3}(1+u)^2t^3/6}$$

$$= \frac{2\Gamma(1/3)\cos(\pi/6)}{3}\left[\frac{6}{\omega_b^{o3}(1+u)^2}\right]^{1/3} . \qquad (A7)$$

In this case the resonance occurs at y=t=0, where $\psi_s=0$.

(iii) For $\tilde{\Omega} > k$ the stationary phase point occurs at

$$\omega_b t_s = \ell n\left[\frac{1+iR\ \tanh(\beta_s/2)}{1-iR\ \tanh(\beta_s/2)}\right] = 2i\alpha_s ,$$

with $\tan\alpha_s = R\ \tanh(\beta_s/2)$ and $\beta_s = -\cosh(\tilde{\Omega}/k)$. The stationary phase point t_s is always closer to real t axis than the nearest branch point as shown in Fig. 7.

The stationary phase contribution gives

$$A_k(\Omega,u) = \frac{1}{\omega_b^o}\exp\{-k\beta_s - 2(\omega''/\omega_b)\tan^{-1}[R\ \tanh(\beta_s/2)]\} \times \left[\frac{2\pi}{\Omega(\tilde{\Omega}^2/k^2-1)^{1/2}}\right]^{1/2} . \qquad (A8)$$

For $\tilde{\Omega} >> k$ the result simplifies using $\beta_s = \ell n(2\tilde{\Omega}/k) > 1$ and $\tanh(\beta_s/2) \simeq 1$ to

$$A_k(\Omega,u) = \frac{2}{\omega_b^o}\left(\frac{2\pi}{\Omega}\right)^{1/2}\left(\frac{2\Omega}{k}\right)^{k-1}\exp\{-2(\omega''/\omega_b)\tan^{-1}R\} . \qquad (A9)$$

For the special case u=0 the orbit[4] 2y(t) is the pendulum orbit and the result (A9) agrees with that of Chirikov in his Eq. (A.11) with k=m and $\tan^{-1}R = \pi/4$. For $u \to 1$, $\tan^{-1}R \simeq R$ and the exponent in Eq. (A9) becomes $\exp(-\omega''/\omega_b^o)$.

The stationary phase integrals show that the effective range of the strong interaction time intervals τ_{int} are given by (i) $\tau_{int} = 1/(\omega_b^o\omega'')^{1/2}$, (ii) $\tau_{int} = 1/(\omega_b^o\omega''^2)^{1/3}$ and (iii) $\tau_{int} = 1/|\omega''|$.

Figure Captions

1. Contours of constant electrostatic potential, $\underset{\sim}{E}\times\underset{\sim}{B}$ flow and the action integral.
2. Integrable $\underset{\sim}{E}\times\underset{\sim}{B}$ flow in a single drift wave given by Eq. (13).
3. Effect of 10% secondary drift wave, Eqs. (18)-(20), on the integrable flow as the frequency of the perturbation is varied through the resonance condition (22).
4. Destruction of the islands in the special four wave system in Sec. IIIB constructed to have a fixed point in the E×B flow.
5. Breakdown of the bounding surfaces and the onset of diffusion as a function of wave amplitude Φ_1 for the example in Sec. IV.
6. Measured diffusion as a function of wave amplitude Φ_1 compared with the theoretical scalings of Φ_1^2 and Φ_1 given in Sec. IV.
7. Contours of integration in the complex t plane used in the evaluation of the Melnikov-Arnold integral.

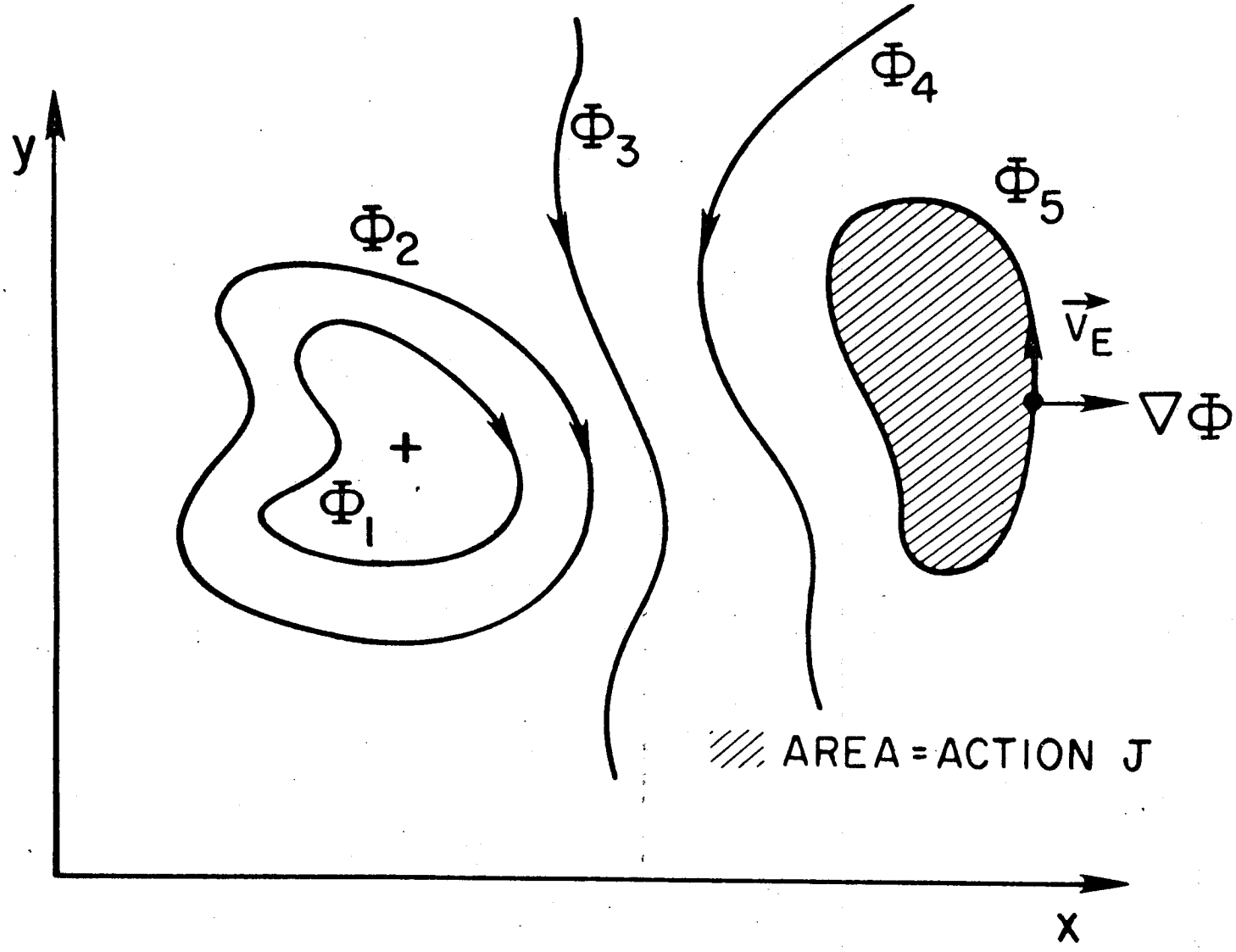

FIG. 1

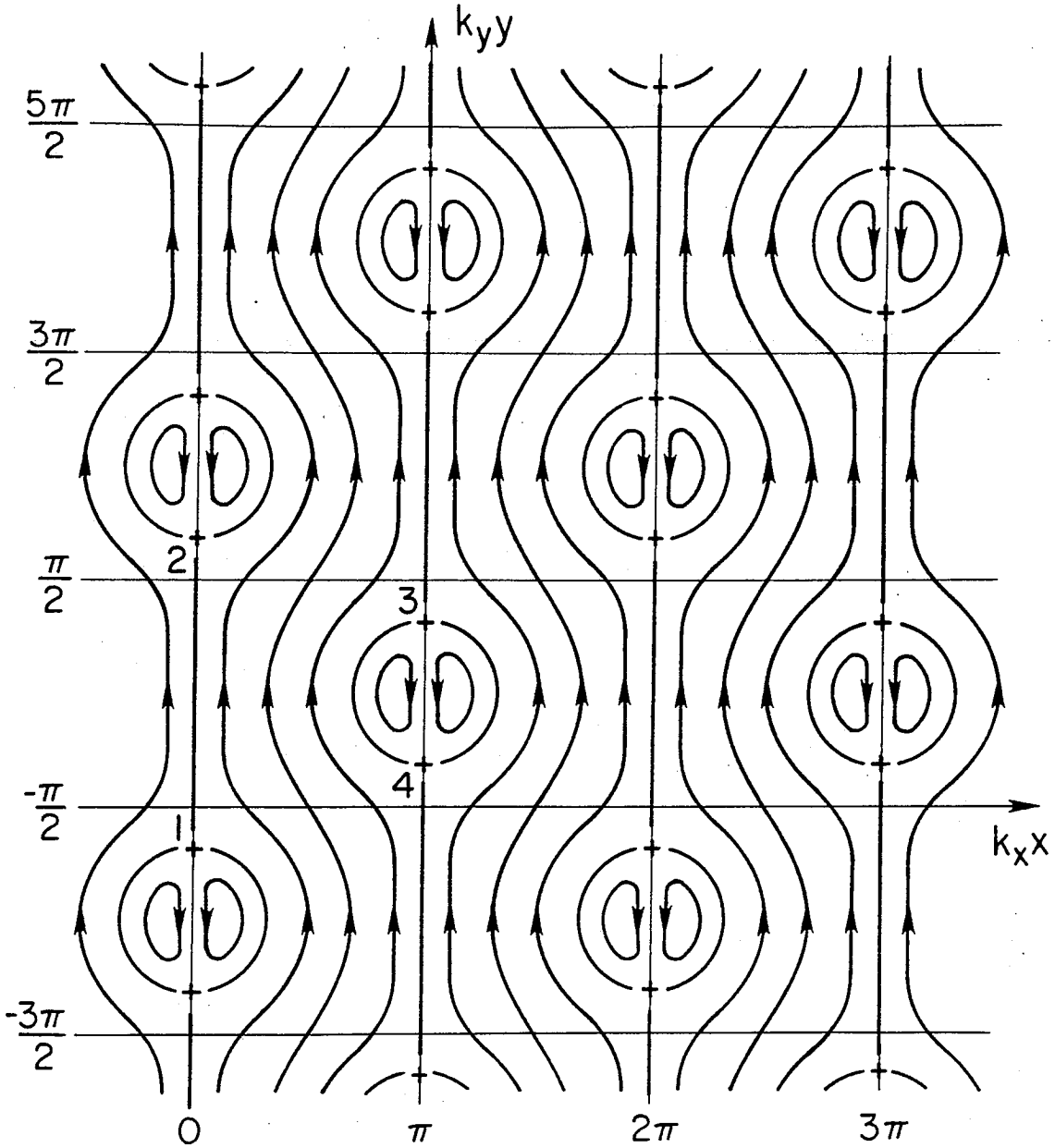
$k_y y$
$\frac{5\pi}{2}$
$\frac{3\pi}{2}$
$\frac{\pi}{2}$
$\frac{-\pi}{2}$
$\frac{-3\pi}{2}$
1
2
3
4
$k_x x$
0
π
2π
3π

FIG. 2

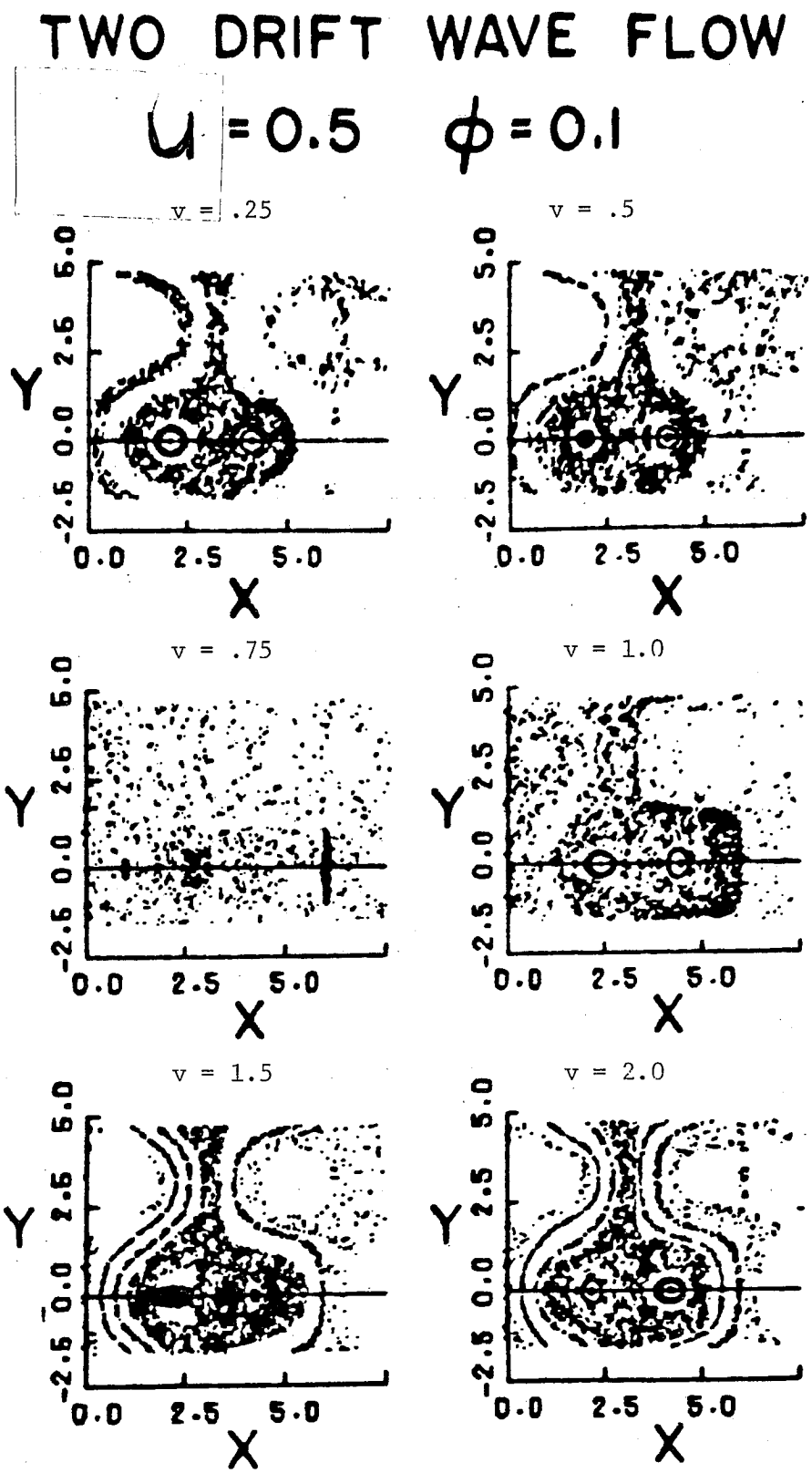
TWO DRIFT WAVE FLOW
U = 0.5 φ = 0.1
v = .25
v = .5
v = .75
v = 1.0
v = 1.5
v = 2.0
Y
X
5.0
2.5
0.0
-2.5
0.0
2.5
5.0

FIG. 3

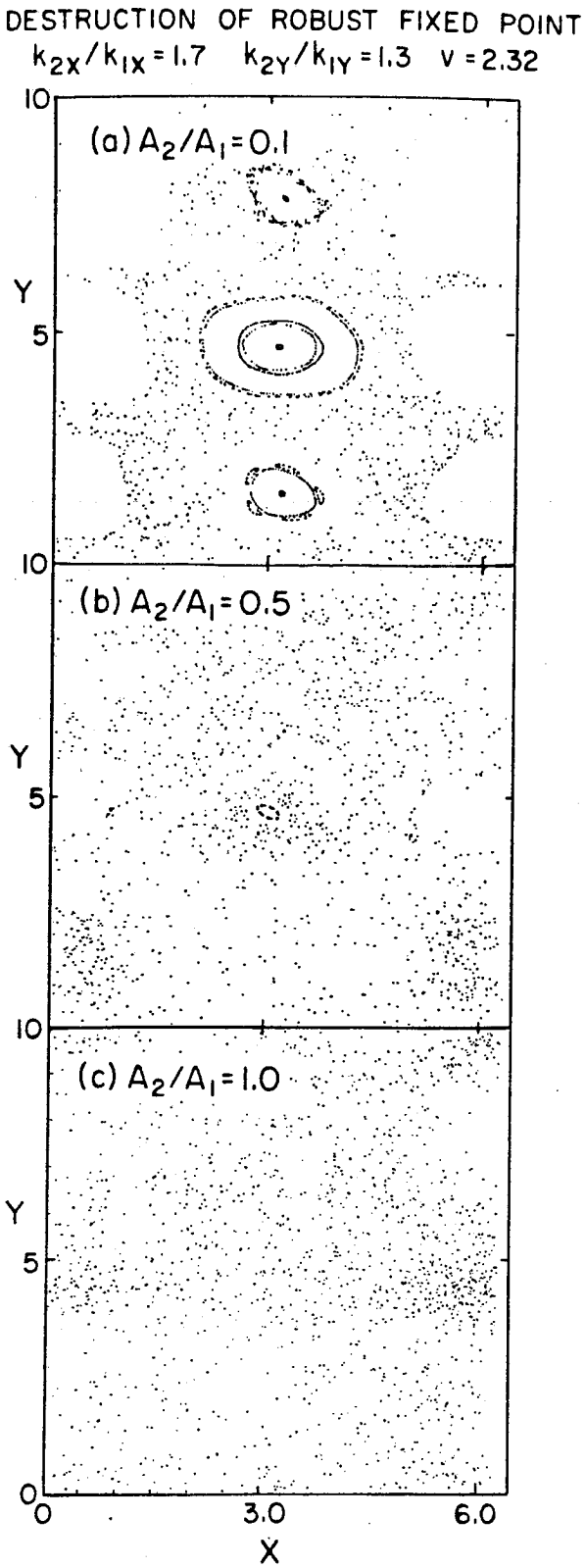
DESTRUCTION OF ROBUST FIXED POINT
$k_{2X}/k_{1X}=1.7$ $k_{2Y}/k_{1Y}=1.3$ $v=2.32$
(a) $A_2/A_1=0.1$
(b) $A_2/A_1=0.5$
(c) $A_2/A_1=1.0$
Y
X
0
3.0
6.0
5
10

FIG. 4

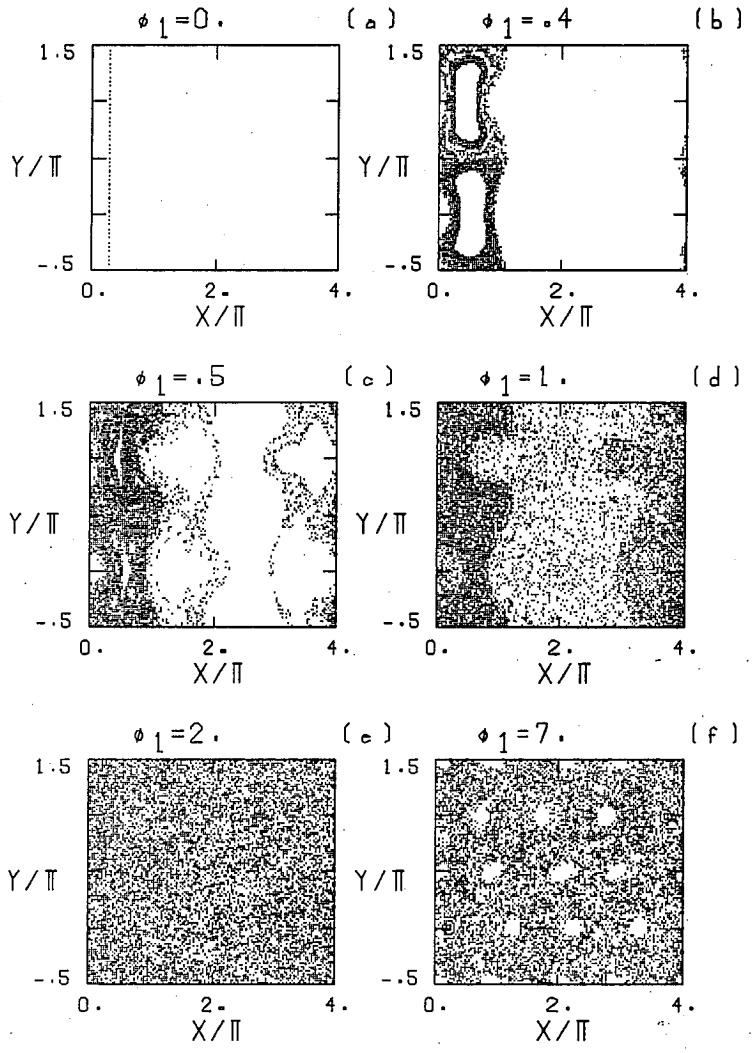

Fig.5

ρ=0

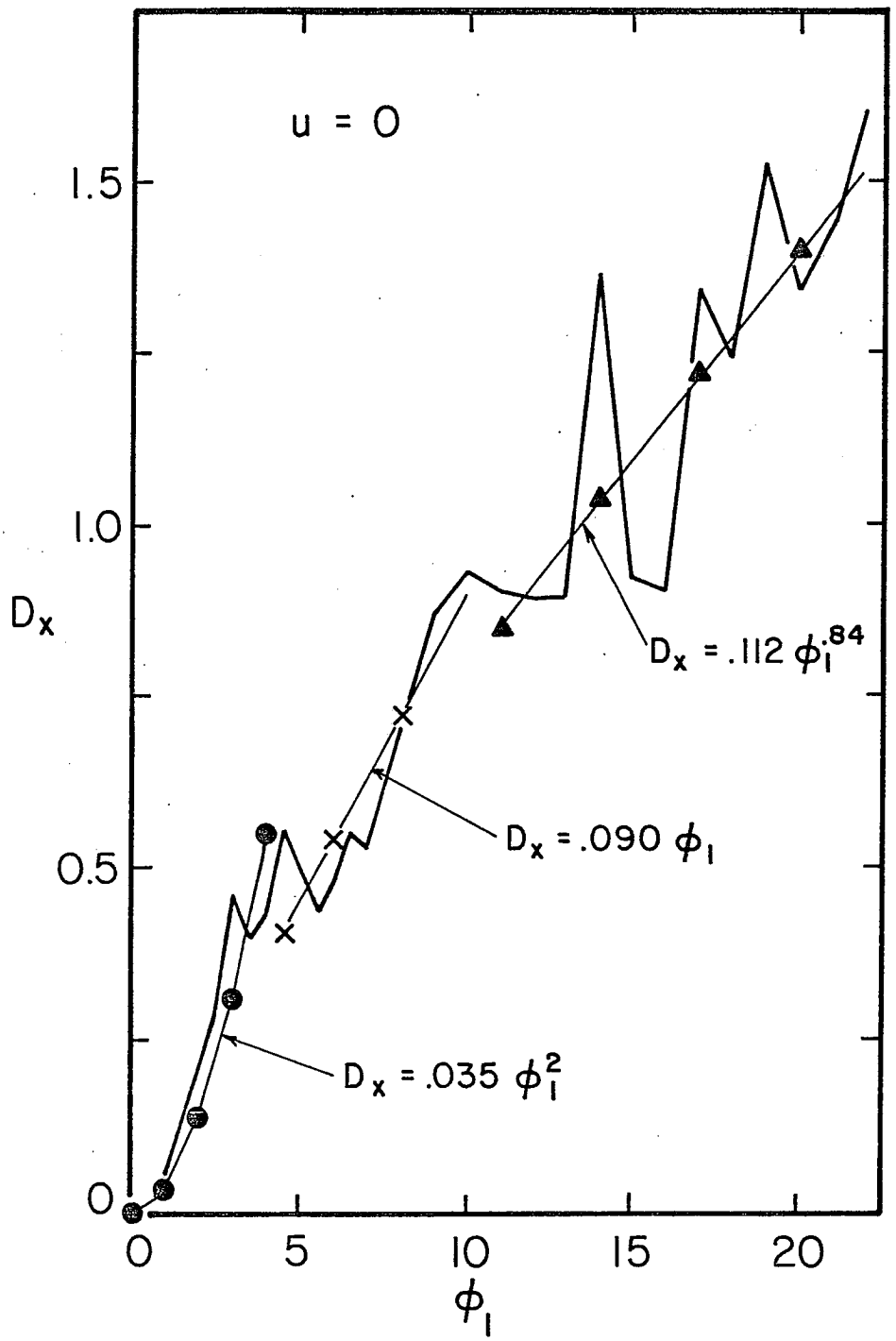
u = 0
1.5
1.0
0.5
0
D_x
$D_x = .112\ \phi_1^{.84}$
$D_x = .090\ \phi_1$
$D_x = .035\ \phi_1^2$
0
5
10
15
20
ϕ_1

FIG. 6a

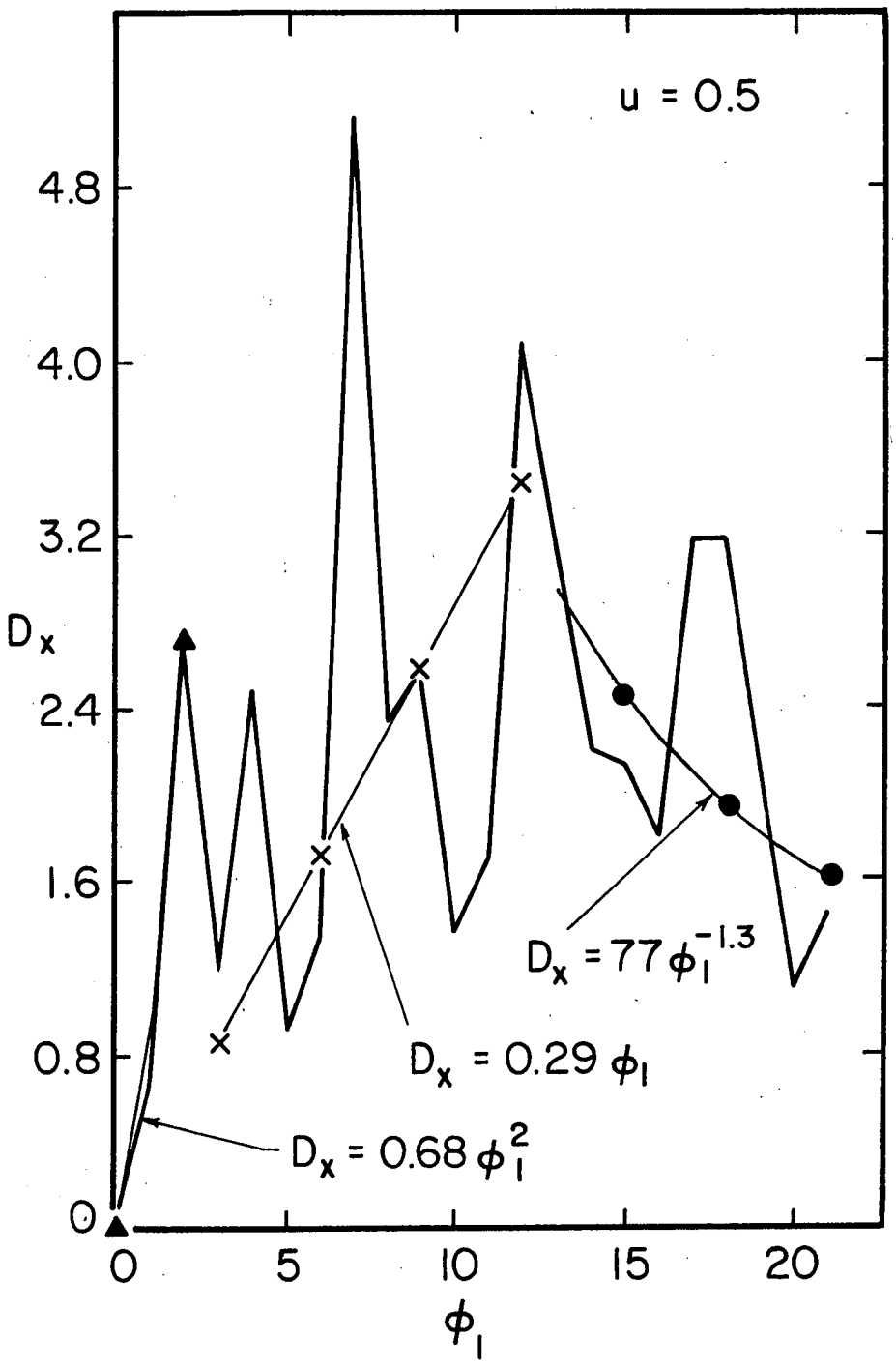
u = 0.5
4.8
4.0
3.2
2.4
1.6
0.8
0
D_x
0
5
10
15
20
ϕ_1
$D_x = 77\,\phi_1^{-1.3}$
$D_x = 0.29\,\phi_1$
$D_x = 0.68\,\phi_1^2$

FIG. 6b

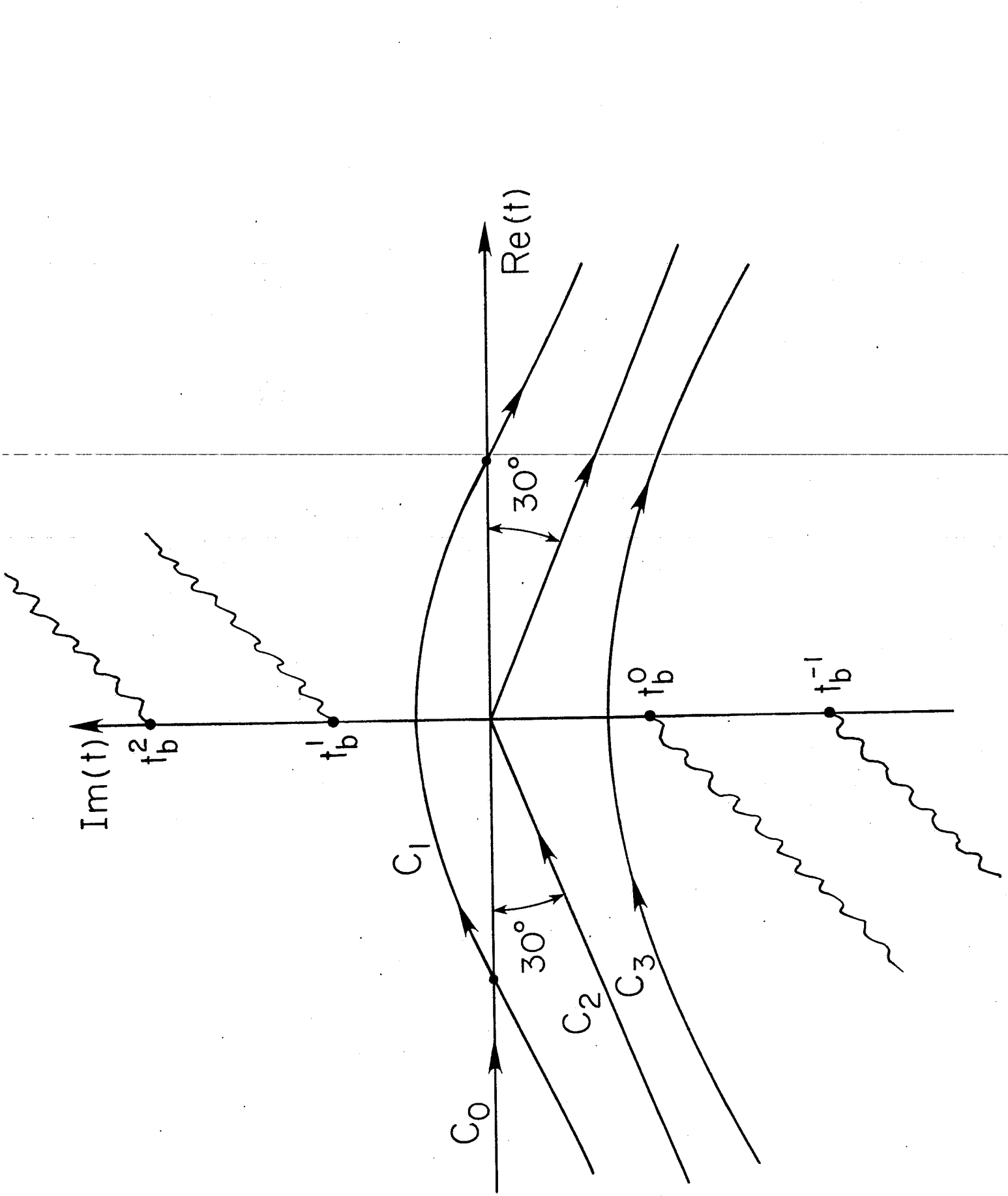

FIG. 7

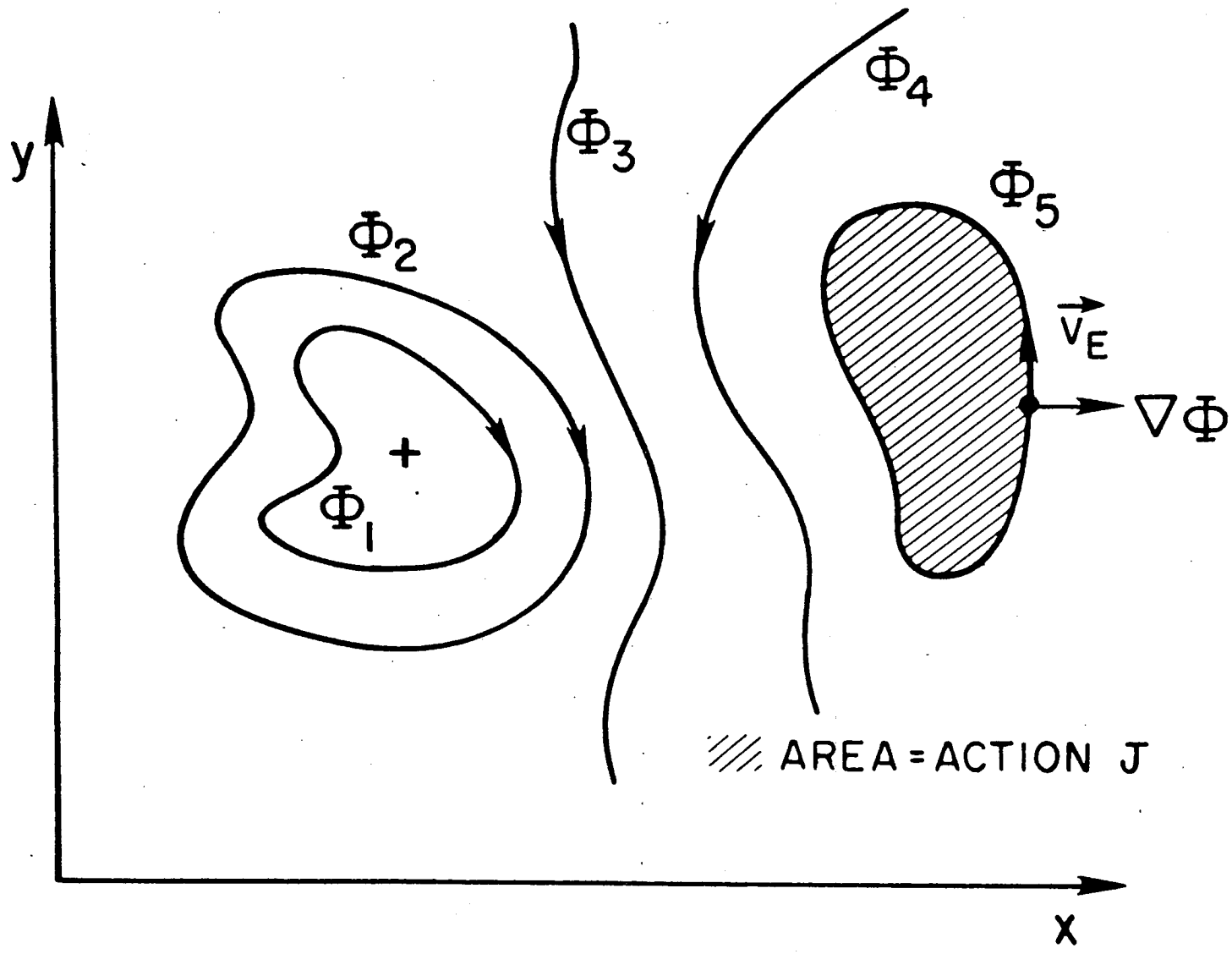

FIG. 1

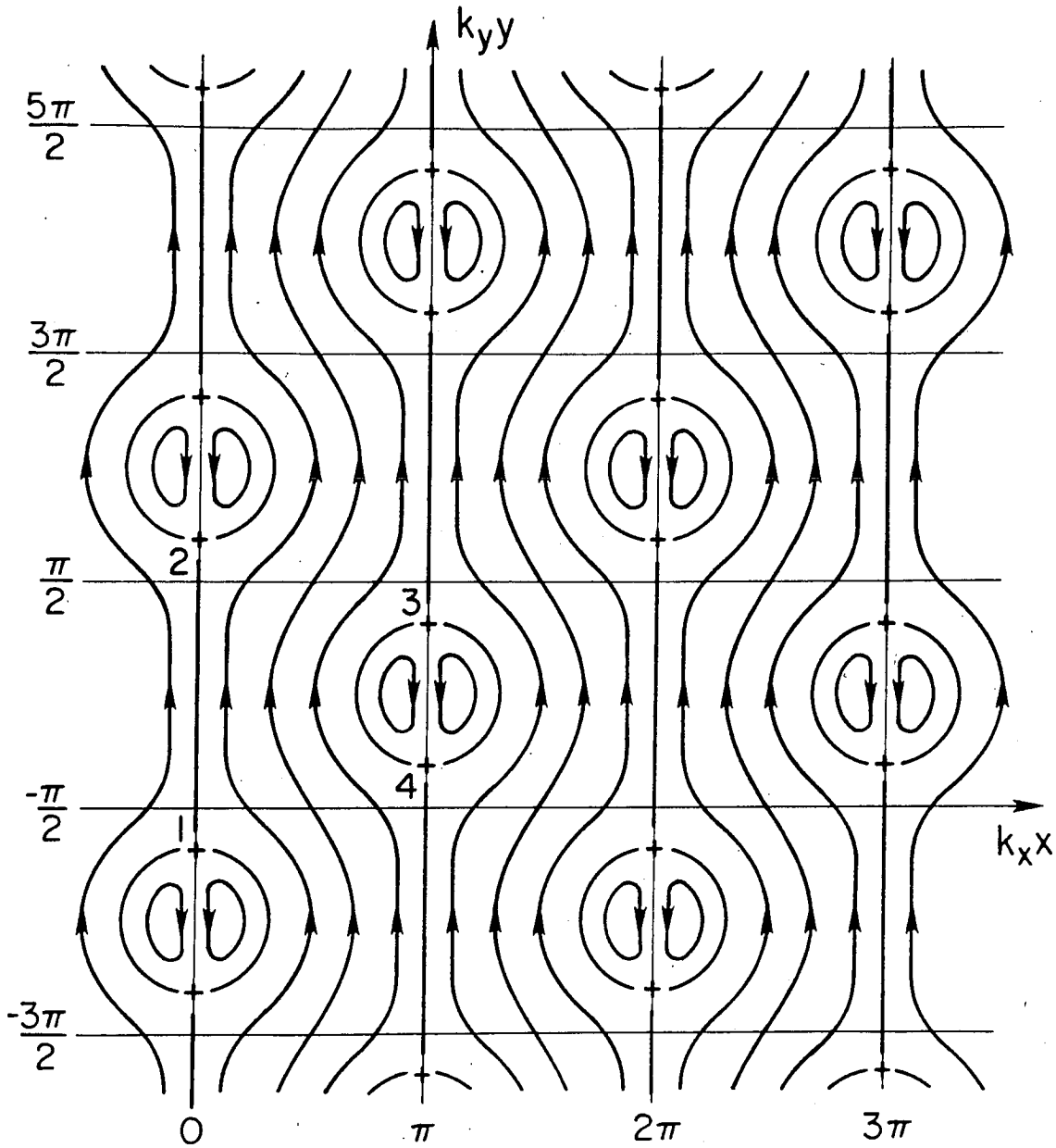
$k_y y$
$\frac{5\pi}{2}$
$\frac{3\pi}{2}$
$\frac{\pi}{2}$
$-\frac{\pi}{2}$
$-\frac{3\pi}{2}$
1
2
3
4
$k_x x$
0
π
2π
3π

FIG. 2

TWO DRIFT WAVE FLOW

$U = 0.5 \quad \phi = 0.1$

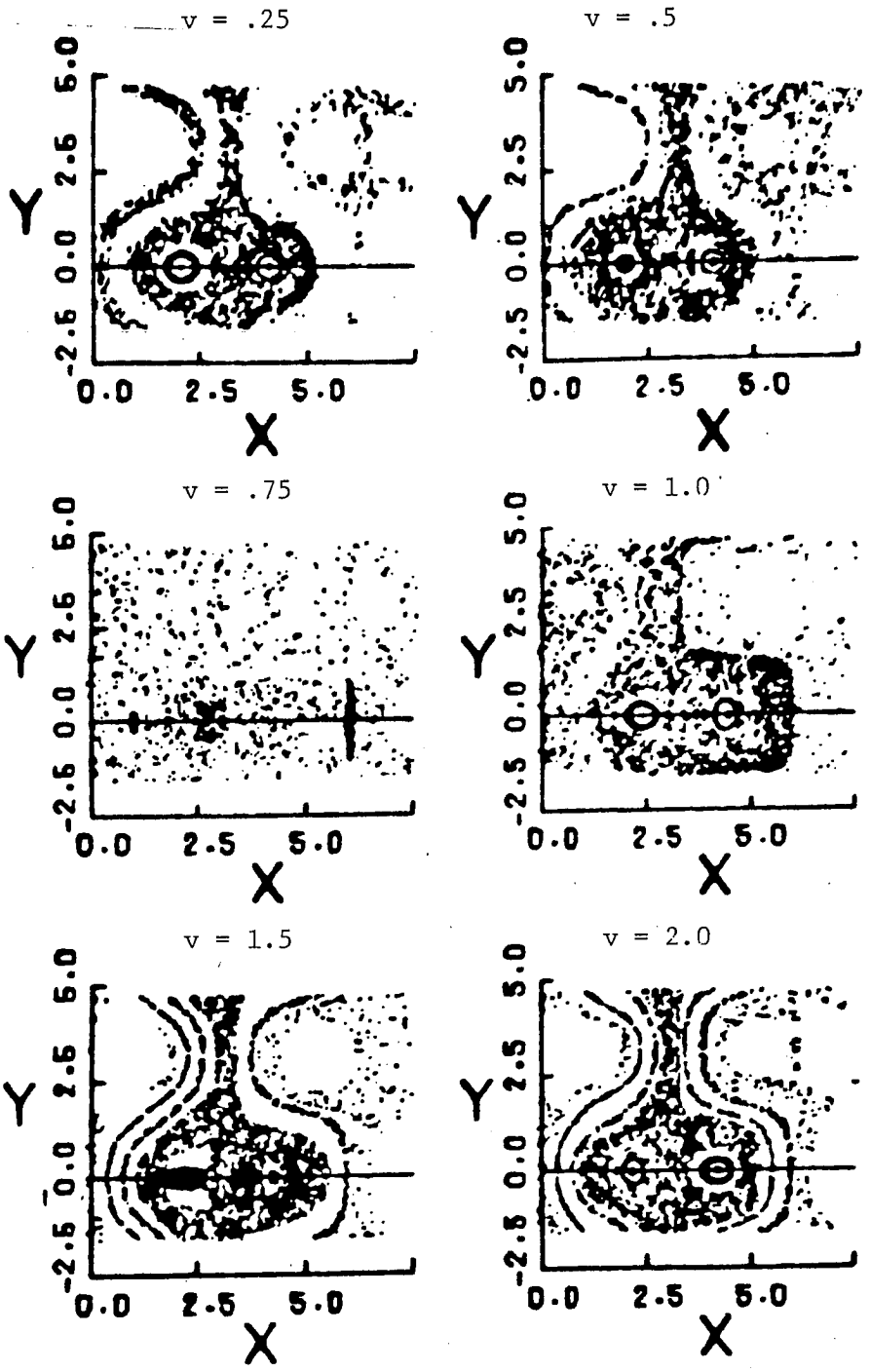

FIG. 3

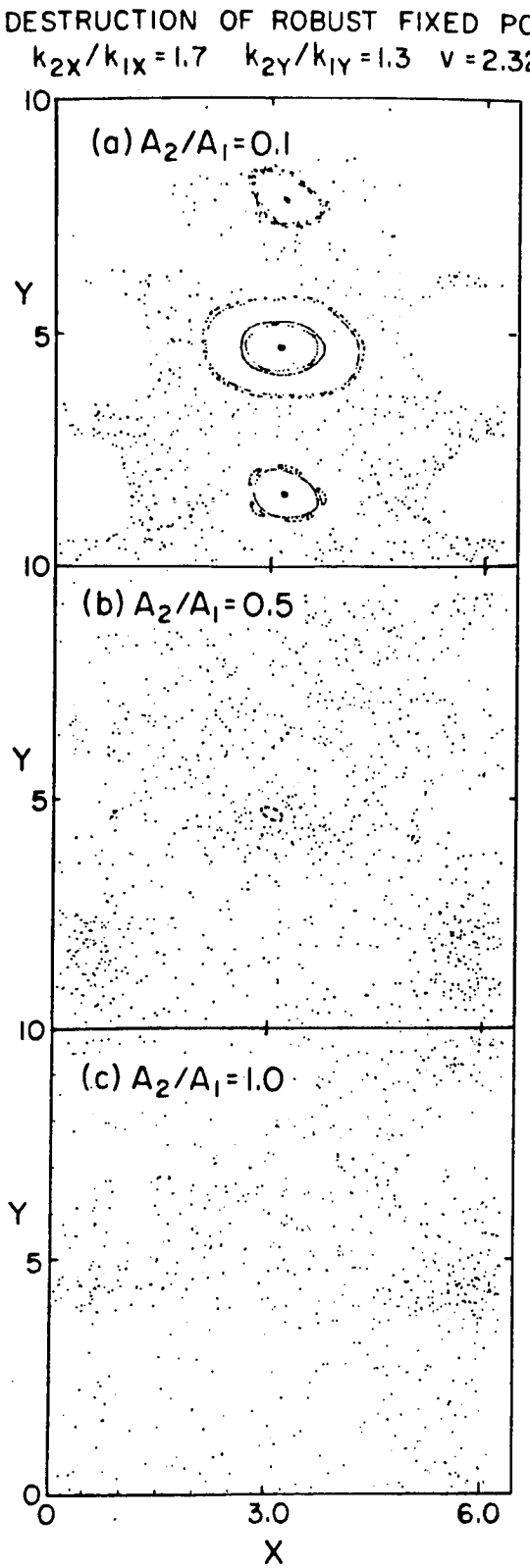
DESTRUCTION OF ROBUST FIXED POINT
$k_{2X}/k_{1X} = 1.7$ $k_{2Y}/k_{1Y} = 1.3$ $v = 2.32$
(a) $A_2/A_1 = 0.1$
(b) $A_2/A_1 = 0.5$
(c) $A_2/A_1 = 1.0$
Y
X
10
5
0
3.0
6.0

FIG. 4

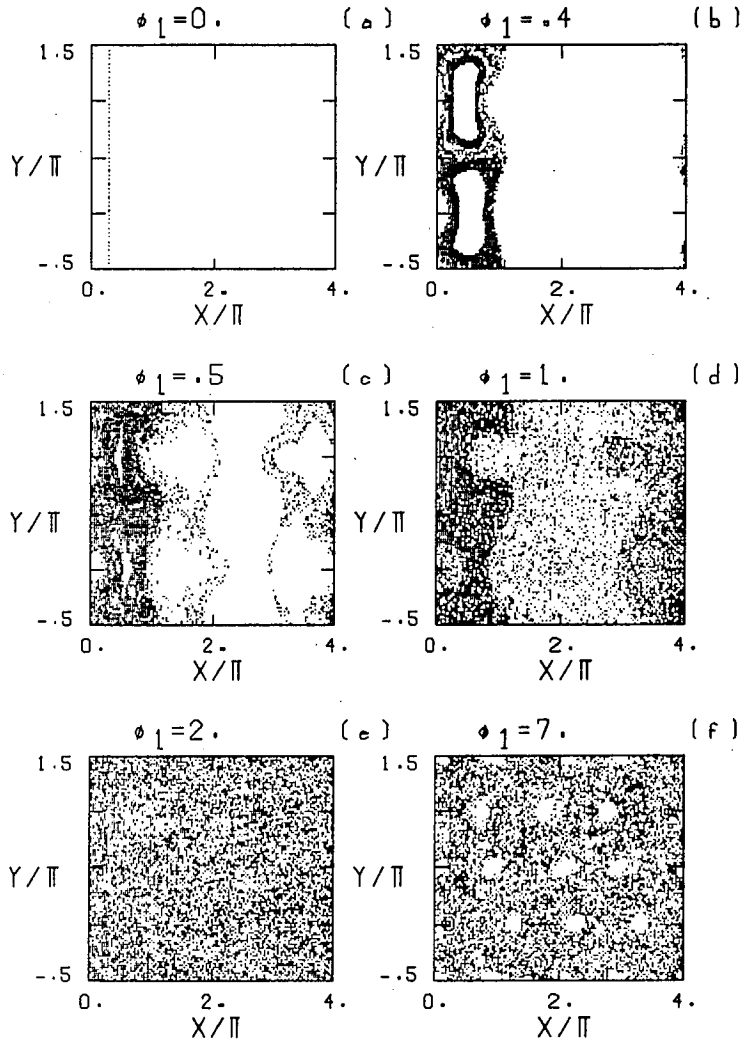

Fig.5

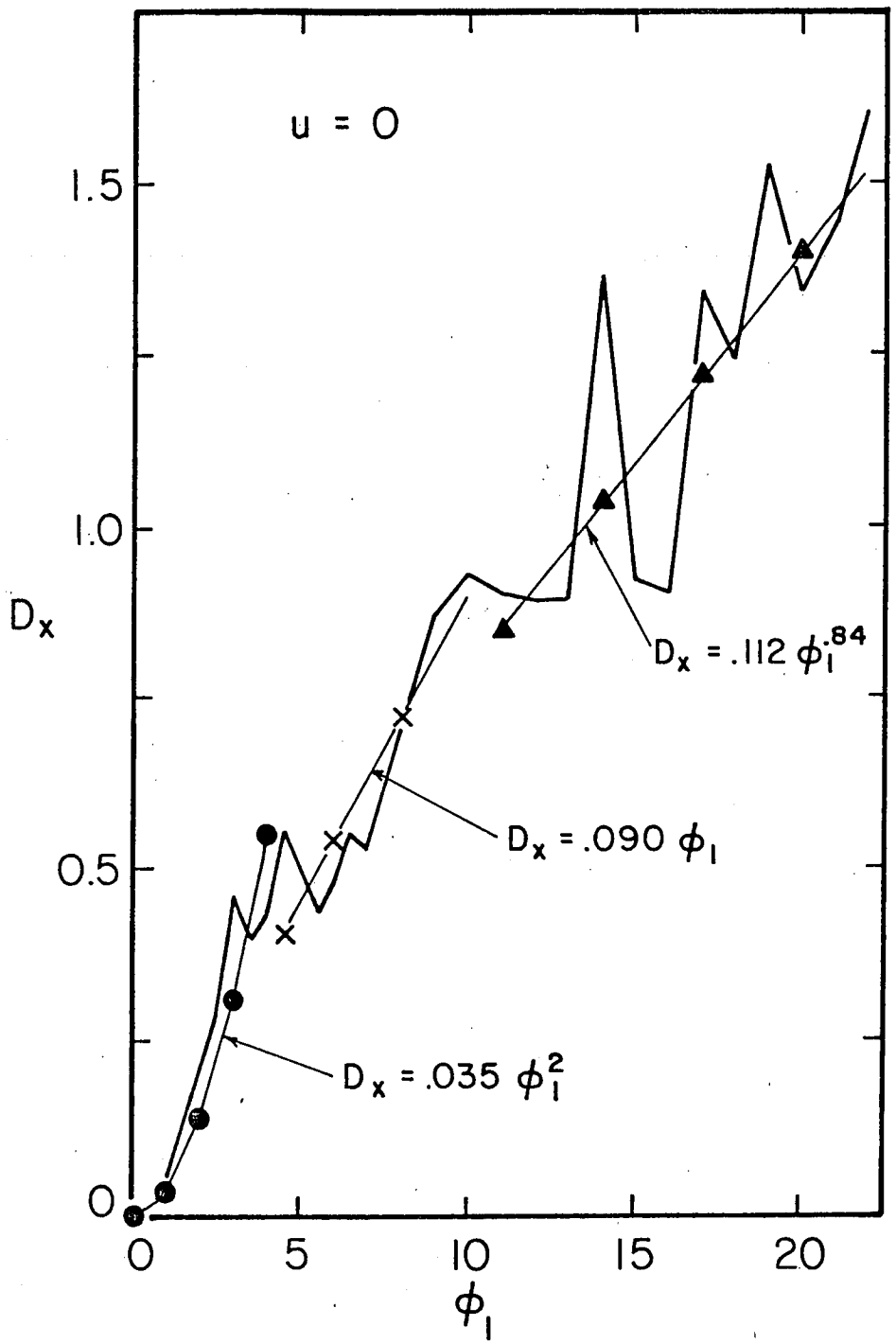
u = 0
1.5
1.0
0.5
0
D_x
$D_x = .112\ \phi_1^{.84}$
$D_x = .090\ \phi_1$
$D_x = .035\ \phi_1^2$
0
5
10
15
20
ϕ_1

FIG. 6a

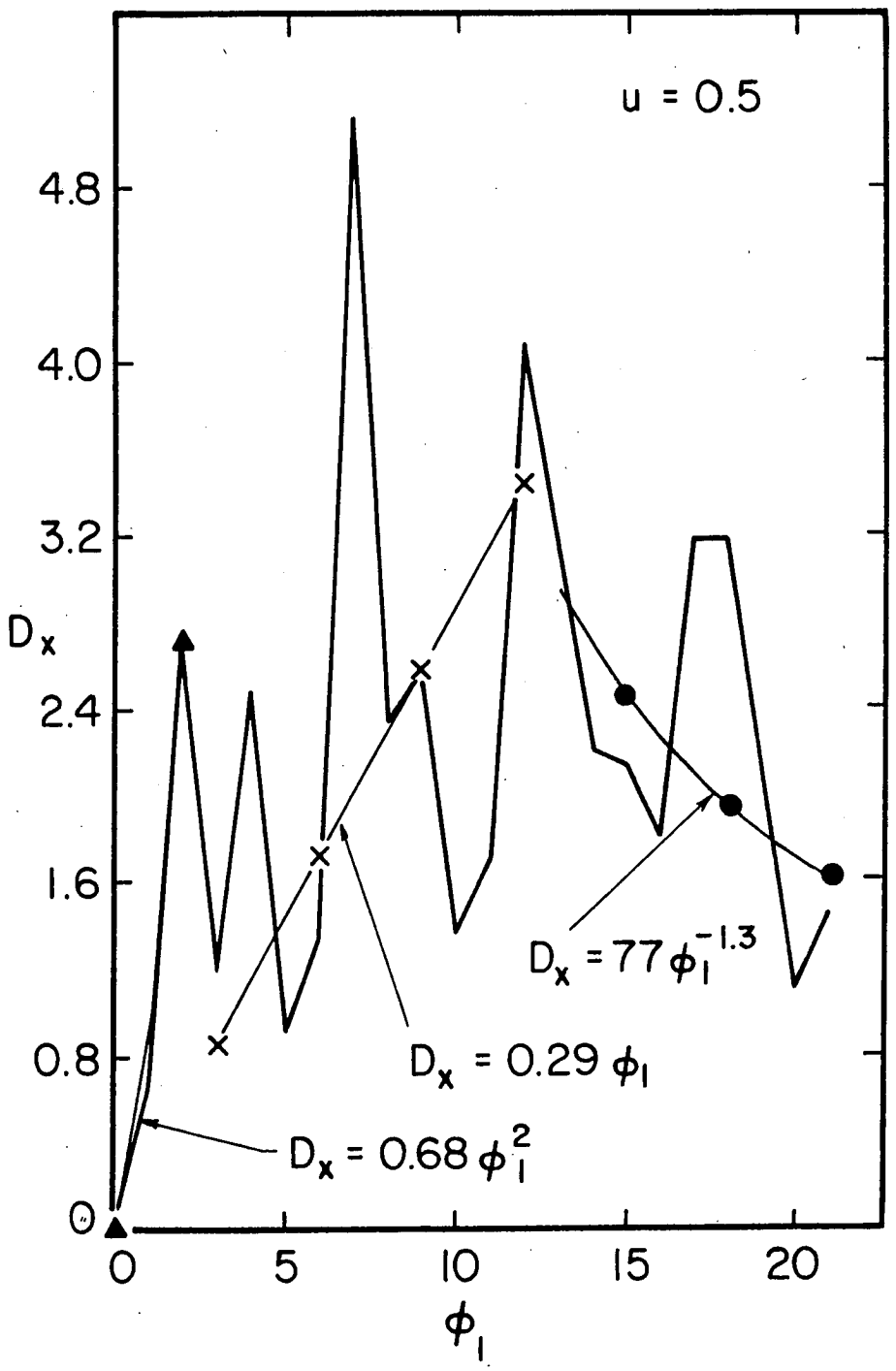
u = 0.5
4.8
4.0
3.2
2.4
1.6
0.8
0
D_x
0
5
10
15
20
ϕ_1
$D_x = 77\,\phi_1^{-1.3}$
$D_x = 0.29\,\phi_1$
$D_x = 0.68\,\phi_1^2$

FIG. 6b

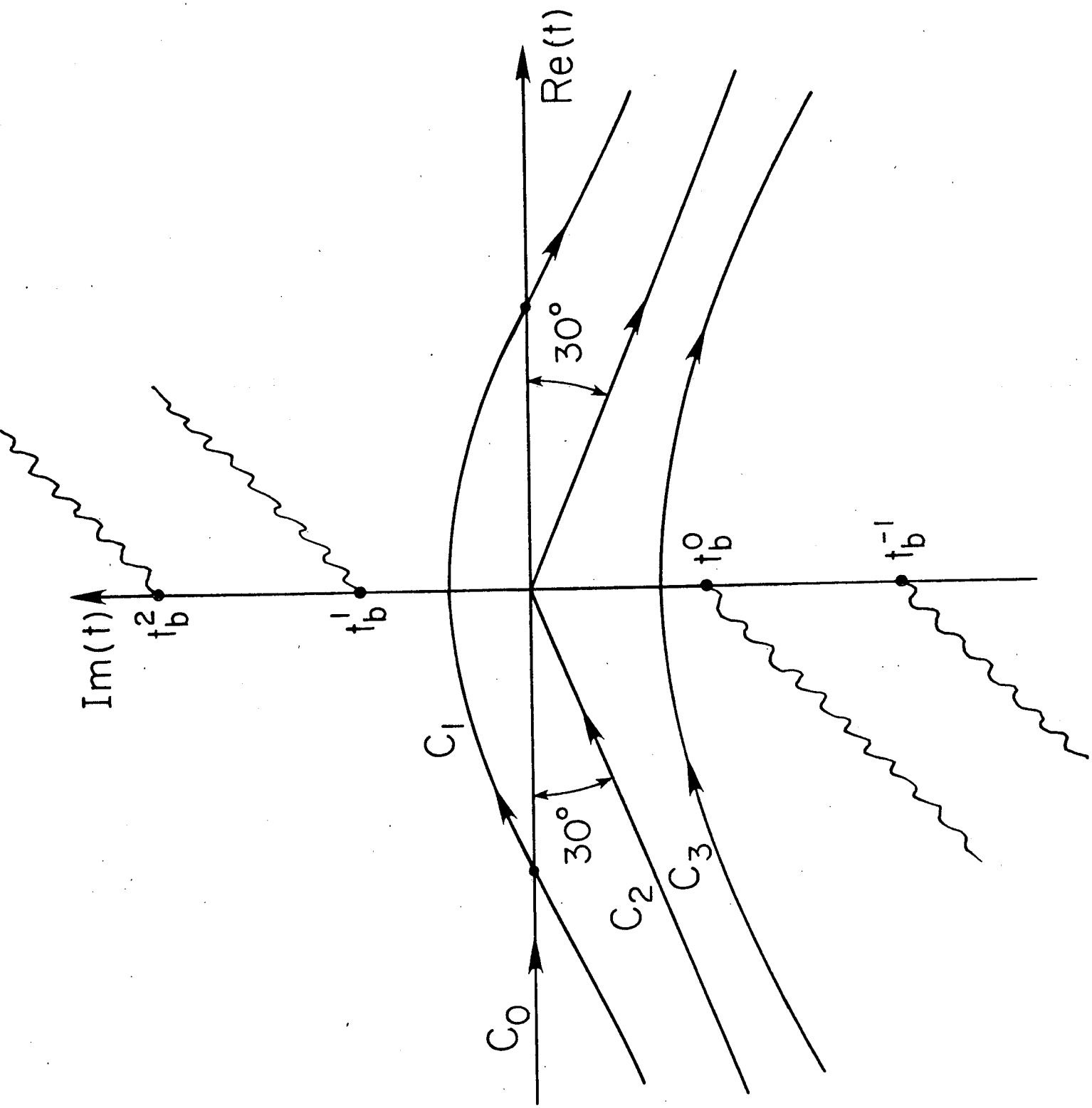

FIG. 7